

## Systematization of the stable crystal structure of all $AB$ -type binary compounds: A pseudopotential orbital-radii approach

Alex Zunger

Solar Energy Research Institute, Golden, Colorado 80401

(Received 12 June 1980)

We discuss the role of the classical crossing points of the nonlocal density-functional atomic pseudopotentials in systematizing the crystal structures of all binary  $AB$  compounds (with  $A \neq B$ ). We show how these pseudopotential radii  $\{r_i\}$  can be used to "predict" the stable crystal structure of all known (565) binary compounds. We discuss the correlation between  $\{r_i\}$  and semiclassical scales for bonding in solids.

### I. INTRODUCTION

Our experience in understanding the occurrence of a large variety of crystal structures in nature has been traditionally expressed in two general frameworks: variational quantum mechanics and a semiclassical approach. The bulk of our experience in understanding the structural properties of molecules and solids from the quantum-mechanical viewpoint is expressed in terms of constructs originating from the calculus of variation: total energy minimization, optimum subspaces of basis functions, etc. In this approach, one constructs a quantum-mechanical-energy functional representing the Born-Oppenheimer surface of a compound; its variational minimum in configuration space  $\{\vec{R}\}$  is then sought, usually by first reducing the problem to a single-particle-like Schrödinger equation. The elementary constructs defining this energy functional—the inter-electronic effective potential  $V_{ee}(\vec{r}, \vec{r}')$  and the electron-core potential  $V_{ec}(\vec{r}, \vec{R})$ —can be treated at different levels of sophistication (e.g., semiempirical tight-binding, Thomas-Fermi, Hartree-Fock, density-functional, pseudopotential, etc.). Similarly, a number of choices exist for the wave-function representation (e.g., the Bloch and molecular-orbital representations or the Wannier and valence-bond models, etc.). This approach has become increasingly refined recently, producing considerable detailed information and insight into the electronic structure of molecules (e.g., Refs. 1 and 2) and simple solids (e.g., Ref. 3).

The semiclassical approach to crystal and molecular structure, on the other hand, involves the construction of phenomenological scales ("factors") on which various aspects of bonding and structural characteristics are measured. These include chemical, crystallographic, and metallurgical constructs, such as the electronegativity, the geometry and size factors, the coordination-number factor, the average-electron-

number factor, the orbital-promotion-energy factor, etc.<sup>4</sup> These factors are then represented by various quantitative scales (bond-order, elemental work-function, ionic, metallic, and covalent radii, electronegativity scales, etc.) that are used to deductively systematize a variety of structural properties. Such intuitive and often heuristic scales have had enormous success in rationalizing a large body of chemical and structural phenomena, often in an ingenious way.<sup>5-9</sup> More recently, these semiclassical scales have been used in *quantitative* models, such as the semiempirical valence force field method<sup>10,11</sup> and Miedema's heat-of-formation model,<sup>9</sup> where the remarkable predictive power of these approaches has been demonstrated over large data bases (literally hundreds of molecules and solids).

Even before the pioneering studies of Goldschmidt, Pauling, and others, it was known thermodynamically that the structure-determining energy  $\Delta E_s$  of most ordered solids is small compared to the total cohesive energy  $\Delta E_0$ . Measured heats of transformation and formation data,<sup>12,13</sup> as well as quantum-mechanical calculations of stable and hypothetical structures, indicate that  $\Delta E_s/\Delta E_0$  can be as small as  $10^{-3}$ – $10^{-4}$ . This poses an acute difficulty for variational quantum-mechanical models. The elementary constructs of the quantum-mechanical approach,  $V_{ee}(\vec{r}, \vec{r}')$  and  $V_{ec}(\vec{r}, \vec{R})$ , are highly nonlinear functions of the individual atomic orbitals that interact to form the crystalline wave functions (due to both the operator nonlocality of  $V_{ee} + V_{ec}$  and their self-consistent dependence on the system's wave functions). Consequently, the structural energies  $\Delta E_s$  become inseparable from the total energies  $\Delta E_0$ . One is then faced with the situation that the complex *weak interactions*, responsible for stabilizing one crystal structure rather than another, are often masked by errors and physical uncertainties in the calculation of the *strong Coulombic interactions* in the total interaction potentials  $V_{ee}(\vec{r}, \vec{r}')$  and  $V_{ec}(\vec{r}, \vec{R})$ . Even though  $\Delta E_s$  can be

calculated using quantum mechanics with the aid of large computers (for sufficiently simple systems), it is notable that the extent and complexity of the information included in  $V_{ee}(\vec{r}, \vec{r}')$  and  $V_{ec}(\vec{r}, \vec{R})$  far exceeds that required to characterize a crystal structure. For example, although the 12 transition metals Sc, Ti, V, Cr, Fe, Y, Zr, Nb, Mo, Hf, Ta, and W have distinctly different quantum-mechanical effective potentials and are characterized by systematically varying cohesive energies  $\Delta E_0$ , all of them appear in the same bcc crystal form as elemental metals.

Despite this, the crystal structures of a number of *elemental* solids have been successfully described by simple quantum-mechanical approaches. These include the work of Deegan *et al.*<sup>14</sup> in which the stable phase of the elemental transition metals was correlated with the sum of single-particle band energies of model fcc and bcc densities of states, as well as the density-functional pseudopotential approach of Moriarty<sup>15</sup> in which a pseudopotential perturbation theory and a linearized exchange and correlation superposition approximation were used to calculate binding and structural energies of a number of non-transition-element solids. The pseudopotential formalism has also been used by Inglesfield<sup>16</sup> to calculate the alloying behavior of a number of binary systems, emphasizing the electrochemical charge-transfer energy which is described in terms of the difference in the elemental screened pseudopotentials.

A number of other approaches have been used to calculate formation energies of binary alloys, neglecting the structural-energy contributions  $\Delta E_s$ . These include the tight-binding approaches of Friedel,<sup>17</sup> Cyrot and Cyrot-Lackmann,<sup>18</sup> Hodges,<sup>19</sup> Pettifor,<sup>20</sup> and Varma<sup>21</sup> in which the shift in the alloy *d*-band density of states with respect to that of its constituent elemental metals is correlated with the heat of formation. The various contributions to this energy difference are calculated by moment approaches and charge-transfer effects are either approximated simply<sup>18,20</sup> or argued to be small.<sup>19</sup> The chemical-potential method of Alonso and Girifalco<sup>22</sup> focuses on the positive contribution to the formation energy arising from the elimination of the density mismatch at the cell boundaries of the constituent elemental metals and the negative contribution originating from a chemical-potential equalization through charge transfer (described by the nonlocality of the atomic pseudopotentials).

These approaches have successfully described the dominance of the *d*-electron contributions to the regularities in elemental crystal structures and cohesive energies and some of the systematics

of compound heat of formation. However, they have not isolated the key physical factors underlying the *structural regularities of nonelemental compounds* (i.e., *AB* with  $A \neq B$ ). It appears that at present, the quantum-mechanical approach seems to lack the simple *transferability* of structural constructs from one system to the other, as well as the *physical transparency* required to assess the origin of structural regularities. The semiclassical approach, on the other hand, concentrates on the construction of physically simple and transferable coordinates that may systematize directly the trends underlying the structural energies  $\Delta E_s$ . The major limitations of the semiclassical approach seem to lie in the occurrence of internal linear dependencies among the various structural factors (e.g., orbital electronegativity and orbital promotion energy), as well as in the appearance of a large number of crystalline structures placed within narrow domains of the phenomenological structural parameters (e.g., Mooser-Pearson plots for nonoctet *AB* compounds or diagrams of the frequency of occurrence of a given structure versus average electron-per-atom ratio). Even so, the semiclassical approaches provide valuable insight into the problem because they point to the underlying importance of establishing system-invariant *energy scales* (e.g., electronegativity, promotion energy) as well as *length scales* (e.g., covalent, metallic, and ionic radii).

For the 50–60 non-transition-metal binary octet compounds, the problem of systematizing the five crystal structures (NaCl, CsCl, diamond, zinc blende, and wurtzite) has been solved through the use of the optical dielectric electronegativity concept of Phillips and Van Vechten.<sup>23</sup> This concept diagrammatically displays periodic trends when transferable elemental coordinates are used. Such diagrammatic Pauling-type approaches are extended here to include intermetallic transition-metal compounds (a total of 565 compounds).

In this paper, I show that the recently developed first-principles nonlocal atomic pseudopotentials provide nonempirical energy and length scales. By using a dual and transferable coordinate system derived from these scales, one is able to topologically separate the crystal structures of 565 binary compounds (including simple and transition-metal atoms) with a surprising accuracy. At the same time, these quantum-mechanically derived pseudopotentials allow one to conveniently define the elementary constructs,  $V_{ee}(\vec{r}, \vec{r}')$  and  $V_{ec}(\vec{r}, \vec{R})$ , and use them in detailed electronic-structure calculations for molecules, solids, and surfaces. As such, this approach may provide a step in bridging the gap between the quantum-mechanical and semiclassical approaches to elec-

tronic and crystal structure.

The success of this approach in correctly "predicting" the structural regularities of as many as 565 binary compounds using elemental coordinates that pertain directly only to the  $s$  and  $p$  electrons (and only indirectly to the  $d$  electrons through the screening potential produced by them) presents a striking result: It suggests that the *structural part*  $\Delta E_s$  of the cohesive energy may be dominated by the  $s$ - $p$  electrons.

This points to the possibility that, while the relatively localized  $d$  electrons determine both *central cell effects* (such as octahedral ligand field and Jahn-Teller stabilizations) and the regularities in the structure-insensitive cohesive energy  $\Delta E_0$  of crystalline and liquid alloys, the longer range  $s$ - $p$  wave functions are responsible for stabilizing one complex space-group arrangement rather than another. There is a striking resemblance between this result and the semiclassical ideas indicating a correlation between the stable crystal structure of transition-metal systems and the number of  $s$  and  $p$  electrons, put forward by Engel<sup>24,25</sup> in 1939 and subsequently greatly refined by Brewer.<sup>26</sup> In the Engel-Brewer approach, the  $d$  electrons play an important but indirect role in determining the energy required for exciting the ground atomic configuration to one that has available for bonding a larger number of unpaired  $s$  and  $p$  electrons. The Engel-Brewer approach has enabled the extension of the Hume-Rothery rules to transition-metal systems simply by counting only the contributions of  $s$  and  $p$  electrons, and at the same time it has explained the stabilities of the bcc, hcp, and fcc structures of the 33 elemental transition metals, the effects of alloying in multicomponent phase diagrams, as well as pressure effects on crystal-structure stabilities, phenomena yet to be tackled by variational quantum-mechanical approaches.

These conclusions on the crucial *structural* roles played by the  $s$  and  $p$  coordinates should be contrasted with the contemporary quantum-mechanical resonant tight-binding approaches suggested first by Friedel<sup>17</sup> for elemental transition metals and recently extended to compounds by Pettifor,<sup>20</sup> Varma,<sup>21</sup> and others. These approaches emphasize the exclusive role of  $d$  electrons in determining *cohesive properties*.

The plan of this paper is as follows: in Sec. II, we introduce the pseudopotential concept and show how it can be used in general to define atomic parameters that correlate with crystal structures. In Sec. III, we discuss the properties of the first-principles atomic pseudopotentials within the density-functional theory of electronic structure. In Sec. IV, we then show how these atomic pseudo-

potentials can be used to define intrinsic core radii that correlate with a large number of electronic and structural properties of crystals. These radii are then used to systematize diagrammatically the stable crystal structure of 565 binary  $AB$  compounds.

## II. PSEUDOPOTENTIALS AND STRUCTURAL SCALES

Although traditionally the inner core orbitals and the outer valence orbitals are treated on an equal footing in variational calculations of the electronic structure of atoms, molecules, and solids, it was recognized as early as 1935 that a large number of bonding characteristics are rather insensitive to the details of the core states.<sup>27,28</sup> This relative insensitivity is a manifestation of the fact that the interaction energies involved in chemical-bond formation ( $10^{-1}$ – $10$  eV), banding in solids (1–25 eV), or scattering events near the Fermi energy ( $10^{-2}$ – $10^{-3}$  eV) are often much smaller than the energies associated with the polarization or overlap of core states. Many methods treating the quantum structure of bound electrons, nucleons, and general fermions have consequently omitted any reference to the core states, variationally treating only "valence" states [Hückel, complete neglect of differential overlap (CNDO), tight-binding, Hubbard models, optical potentials in nuclear physics, effective potentials in Fermi-liquid theories, empirical valence potentials in atomic physics, etc.]. Clearly, however, if no constraints are placed, such a variational treatment will result in an unphysical lowering of the energy of the valence states into the "empty" core ("variational collapse"). Much of the empirical parametrization characteristic of such methods is implicitly directed to avoid such a pathology. It was first recognized, however, by Phillips and Kleinman<sup>29</sup> that the price for reducing the orbital space to valence states alone can be represented by an additional nonlocal potential term (pseudopotential) in the Hamiltonian.

Although the pseudopotential concept has offered great qualitative insight into the nature of bonding states in polymers and solids (e.g., Ref. 30), its calculation in practical electronic-structure application has generally been avoided.<sup>31-33</sup> Instead, it has been replaced by a local form with disposable parameters adjusted to fit selected sets of data (semiconductor band structures, Fermi surface of metals, atomic term values, etc.). Since the valence electronic energies near the Fermi level are determined (to within a constant) by relatively low-momentum transfer electron-core scattering events ( $|q| \approx 2k_F$ ), it has been possible in the past to successfully describe the one-elec-

tron optical spectra and Fermi surface of many solids assuming pseudopotentials that are truncated to include only small momentum components (i.e., smoothly varying in the core region in configuration space). The freedom offered by the insensitivity of the electronic band-structure dispersion relation  $\epsilon_j(\vec{k})$  to the variations of the pseudopotential in the core region has been exploited to obtain empirical potentials converging rapidly in momentum space and hence amenable to electron-gas perturbative theories<sup>34</sup> and plane-wave-based band-structure calculations.<sup>32,33</sup>

These soft-core empirical pseudopotentials have produced the best fits to date for the observed semiconductor band structures,<sup>31</sup> and their descendants, the soft-core self-consistent pseudopotentials, have yielded the most detailed information on semiconductor surface states.<sup>35</sup> The insensitivity of  $\epsilon_j(\vec{k})$  to the high-momentum components of the pseudopotential has prompted an enormous amount of literature in which different forms for the potential have been suggested (empty cores, square wells, Gaussian-shaped, etc.) all producing reasonable fits to the energy levels near the Fermi energy. Since, however, these pseudopotentials were fitted predominantly to energy levels in atoms and solids (and were not constrained to produce physically desirable wave functions) they often yielded systematic discrepancies with experiment or all-electron calculations of the bonding charge density in molecules and solids.<sup>36-38</sup> Such discrepancies result from the fact that higher-momentum components (e.g.,  $|q| \gtrsim 6k_F$  in crystalline silicon), not included in energy-level-fitted soft-core pseudopotentials, are of importance in determining the directional distribution of the bonding charge density. The striking success of the empirical pseudopotential is that it made it possible to reduce the informational content of the often complex electronic spectra of semiconductors to a few (usually three to five) nearly transferable elemental parameters (empirical pseudopotential form factors). The implied locality of the pseudopotential, as well as its truncation to low-momentum components, however, has limited its chemical content to reflect predominantly the low-energy electronic excitation spectrum rather than explicit structural and chemical regularities.

Recently, Simons<sup>39</sup> and Simons and Bloch<sup>40</sup> have observed that there exists at least one class of *structurally significant* empirical pseudopotentials containing very-high-momentum components (i.e.,  $|q| \gg 2k_F$ , or hard-core pseudopotentials). The general form of a screened pseudopotential is:

$$V_{\text{eff}}^{(l)}(\vec{r}) = V_{\text{ps}}^{(l)}(\vec{r}) + V_{\text{scr}}[n(\vec{r})]. \quad (1)$$

[We use a capital  $V(\vec{r})$  to denote solid-state potentials, while  $v(r)$  will denote atomic or ionic potentials.] Here  $V_{\text{ps}}^{(l)}(\vec{r})$  is the bare pseudopotential acting on the  $l$ th angular momentum wavefunction component, and  $V_{\text{scr}}[n(\vec{r})]$  is the Coulomb, exchange, and correlation screening due to the pseudocharge density  $n(\vec{r})$ . For the simple case of one-electron ions, chosen by Simons and Bloch, the screening potential reduces to zero. The bare atomic pseudopotential  $v_{\text{ps}}^{(l)}(r)$  was then assumed to take a simple hard-core form:

$$v_{\text{eff}}^{(l)}(r) = v_{\text{ps}}^{(l)}(r) = B_l/r^2 - Z_v/r, \quad (2)$$

where  $Z_v$  is the valence charge and the parameter  $B_l$  is adjusted such that the negative of the orbital energies  $\epsilon_{nl}$  obtained from the pseudopotential equation:

$$\left[-\frac{1}{2}\nabla_r^2 + v_{\text{eff}}^{(l)}(r)\right]\psi_{nl}(r) = \epsilon_{nl}\psi_{nl}(r) \quad (3)$$

match the observed ionization energies of one-electron ions such as  $\text{Be}^{+1}$ ,  $\text{C}^{+3}$ ,  $\text{O}^{+5}$ , etc. These hard-core pseudopotentials are characterized by an orbital-dependent crossing point  $r_l^0$  at which  $v_{\text{eff}}^{(l)}(r_l^0) = 0$ . These orbital radii then possess the same periodic trends underlying the observed single-electron ionization energies through the Periodic Table. The remarkable feature of these radii is that they form powerful structural indices, capable of systematizing the various crystal phases of the octet  $A^N B^{8-N}$  non-transition-metal compounds.<sup>41</sup> Such structural plots have been extended by Machlin, Chow, and Phillips<sup>42</sup> very successfully to some 45 nonoctet (non-transition-metal) compounds.

The realization that these empirical orbital radii are characteristic of the atomic cores, and as such are approximately transferable to atoms in various bonding situations, has led to the construction of a number of new phenomenological relations of the form  $G = f(r_l^0)$ , correlating physical observables  $G$  in *condensed phases* with the orbital radii of the constituent *free ions*. Some examples of  $G$  are the elemental metallic work functions, the melting points of binary compounds, and the Miedema coordinates treated by Chelikowsky and Phillips.<sup>43</sup> What has been realized is that the characteristics of an isolated atomic core, reflected in the spectroscopically determined  $l$ -dependent turning points  $r_l^0$  contain the fundamental constructs describing structural regularities in polyatomic systems.<sup>44,45</sup> This can be contrasted with phenomenological electronegativity scales that are based on observables pertaining to the polyatomic systems themselves, such as the thermochemical Pauling scale, the dielectric Phillips-Van Vechten scale, and the Walsh scale.

Since the general atomic pseudopotential  $v_{\text{eff}}^{(l)}(\vec{r})$

of Eq. (1) can be reduced to a simple form with  $v_{s\alpha} = 0$  only for single-electron stripped ions, the empirical Simons-Bloch orbital radii can only be used for atoms for which stripped-ion spectroscopic data exist. This excludes most transition elements, which form a wealth of interesting inter-metallic structures. Yet, even so, the extraction of a bonding scale from data on ions that lack any valence-valence interactions (e.g.,  $C^{+3}$  and  $O^{+5}$ , representing chemical affinities of C and O) may distort the underlying chemical regularities.<sup>39</sup> In addition, the restriction to single-electron species means that the post-transition-series atoms (e.g., Cu, Ag, Au or Zn, Cd, Hg) are treated as having only one and two valence electrons, respectively, much like the alkali and alkaline-earth elements, respectively.<sup>39-42</sup> However, the increase in melting points and heats of atomization and the decrease in nearest-neighbor distances in going from group IIB to IB metals (e.g., Zn-Cu, Cd-Ag, and Hg-Au), as compared with the *opposite trend* in going from group IIA to IA (Ca-K, Sr-Rb, and Ba-Cs), completely eliminates any possibility of Cu, Ag, and Au having effectively a single-bonding electron. Similar indications on the extensive *s-d* and *p-d* hybridization are given by the large bulk of photoemission data on Cu and Ag halides.<sup>46</sup> In keeping with the single-valence-electron restriction, one is also forced to define the *d*-orbital coordinate of the post-transition elements from the lowest *unoccupied* rather than occupied *d* orbital (i.e., *4d* for Cu and Zn, *5d* for Ag and Cd). This may be reasonably faithful to the chemical tendencies of post-transition elements with sufficiently deep occupied *d* orbitals and sufficiently low unoccupied *d* orbitals (e.g., Br, Te, I), but it is questionable for the elements with occupied semicore *d* shells in the vicinity of the upper valence band (e.g., CdS and ZnS). These pathologies can be corrected by empirically adjusting the valence charge  $Z_v$  in Eq. (2) for these elements.<sup>47</sup> Finally, the simple pseudopotential of Eq. (2) is not suitable for electronic-structure studies, as indicated by Andreoni *et al.*,<sup>48,49</sup> because the wave functions of Eqs. (2) and (3) are severely distorted relative to true valence orbitals by the unphysically long-range  $r^{-2}$  tail. This has been corrected by Andreoni *et al.* by replacing the long-range  $B_1/r^2$  term in Eq. (2) with an  $A_1 e^{-\gamma_1 r}/r^2$  term, with the additional parameter  $\gamma_1$  fixed to fit the orbital maxima. This leads to a new set of renormalized orbital radii differing considerably from the Simons-Bloch set.

One is hence faced with the situation that the soft-core empirical pseudopotential<sup>33</sup> can be used to successfully fit the low-energy electronic band structure of solids, but it lacks the structurally

significant turning points (i.e.,  $v_{\text{eff}}(r) = 0$  only at  $r = \infty$ ); whereas the empirical Simons-Bloch<sup>39,40</sup> potentials do not yield a quantitatively satisfactory description of the electronic structure but do yield the correct structural regularities. The approach that we have taken to remedy this situation is to construct a pseudopotential theory from first principles. The first-principles approach allows for the regularities of energy levels and wave function to be systematically built into the atomic pseudopotentials, without appealing to any experimental data. Because no resort is made to simple, single-electron models, transition elements can be treated as easily as other elements, without neglecting the interactions between valence electrons or assuming that the highest-occupied *d* levels belong to a chemically passive core. Furthermore, since the bare pseudopotential  $v_{\text{ps}}^{(1)}(r)$  and the screening  $v_{s\alpha}[n(r)]$  are described in terms of well-defined quantum-mechanical constructs (such as Coulomb, exchange, and correlation interactions, Pauli forces, and orthogonality holes) both the failures and the successes of the theory could be analyzed.

### III. FIRST-PRINCIPLES DENSITY-FUNCTIONAL PSEUDOPOTENTIALS

#### A. Properties of the density-functional pseudopotentials

The first-principles atomic pseudopotentials discussed here are derived from the spin-density-functional formalism.<sup>50-51</sup> They were first derived by Topiol, Zunger, and Ratner<sup>52,53</sup> for the first row atoms and further extended by Zunger and Zunger and Cohen.<sup>54-58</sup> Details of the method of constructing these pseudopotentials, as well as applications, have been previously discussed.<sup>52-58</sup> Here we briefly summarize the results and establish the notation to be used below.

One starts with the all-electron (ae) single-particle equation for a polyatomic system in a density-functional representation (in which core and valence wave functions are treated on the same footing). In this approach, the effective potential  $V_{\text{eff}}^{\text{ae}}(\vec{r})$  is given as a sum of the external potential  $V_{\text{ext}}(\vec{r})$  (e.g., the electron-nuclear attraction potential) and the interelectron screening potential  $V_{s\alpha}^{\text{ae}}[\rho_c + \rho_v]$ . The latter is a functional of the core (*c*) and valence (*v*) charge density  $\rho(\vec{r}) = \rho_c(\vec{r}) + \rho_v(\vec{r})$  and includes the interelectronic Coulomb  $V_{\text{ee}}[\rho(\vec{r})]$ , exchange  $V_x[\rho(\vec{r})]$  and correlation  $V_c[\rho(\vec{r})]$  potentials.<sup>50,51</sup> The eigenstates  $[\psi_j(\vec{r})]$  of the all-electron single-particle equation:

$$\left\{ -\frac{1}{2}\nabla^2 + V_{\text{ext}}(\vec{r}) + V_{s\alpha}^{\text{ae}}[\rho_c(\vec{r}) + \rho_v(\vec{r})] \right\} \psi_j(\vec{r}) = \epsilon_j \psi_j(\vec{r}) \quad (4)$$

are normally constrained to be orthogonal (and therefore have nodes) and form the basis for expanding the self-consistent charge density

$$\rho(\vec{r}) = \sum_j |\psi_j(\vec{r})|^2.$$

In the pseudopotential representation, one seeks to replace the external potential  $V_{\text{ext}}(\vec{r})$  by a pseudopotential  $V_{\text{ps}}(\vec{r}, \vec{r}')$  such that the lowest eigenstates  $\chi_j(\vec{r})$  have properties of valence, rather than core wave functions. The pseudopotential single-particle equation is hence:

$$\left\{ -\frac{1}{2}\nabla^2 + V_{\text{ps}}(\vec{r}, \vec{r}') + V_{\text{scr}}^{\text{ps}}[n(\vec{r})] \right\} \chi_j(\vec{r}) = \bar{\epsilon}_j \chi_j(\vec{r}), \quad (5)$$

where the valence screening  $V_{\text{scr}}^{\text{ps}}[n(\vec{r})]$  has the same functional form as  $V_{\text{scr}}^{\text{se}}[\rho(\vec{r})]$ , except that it is a functional of the (valence) pseudo-charge-density  $n(\vec{r}) = \sum_j |\chi_j(\vec{r})|^2$ . Since no core states appear below the valence states  $\chi_j(\vec{r})$ , one is free to construct  $\chi_j(\vec{r})$  as nodeless.

One can either attempt to calculate the pseudopotential  $V_{\text{ps}}(\vec{r}, \vec{r}')$  directly for the molecule or solid of interest (i.e., orthogonalized plane-wave-type pseudopotentials), or first to calculate it for a convenient fragment (e.g., atoms, ions) and approximate  $V_{\text{ps}}(\vec{r}, \vec{r}')$  by suitable functions of such transferable quantities  $v_{\text{ps}}(\vec{r}, \vec{r}')$ . The success of the latter approach hinges on the degree of state independence that can be built into the fragments pseudopotential  $v_{\text{ps}}(\vec{r}, \vec{r}')$ : an atomic pseudopotential is useful only to the extent that it continues to produce chemically and physically accurate energies and wave functions even when the atom is placed in bonding environments (e.g., mole-

cules, solids, surfaces) which differ considerably from that characteristic of the species used to construct the pseudopotential (e.g., free atoms or ions). The imposition of explicit physical constraints on the pseudo-wave-functions  $\chi_j(\vec{r})$  leading to an approximately energy- and state-independent (and hence transferable) atomic pseudopotential is central to the present approach.<sup>55, 56, 58</sup> No such considerations were taken in constructing the previous empirical<sup>31-33</sup> or semiempirical<sup>35, 59</sup> pseudopotentials.

The total pseudopotential  $V_{\text{ps}}(\vec{r}, \vec{r}')$  for the polyatomic system is constructed as a superposition of atomic pseudopotentials  $v_{\text{ps}}^{(i)}(\vec{r}) \hat{P}_i$  (where the spatial nonlocality is replaced by an angular momentum dependence through the projection operator  $\hat{P}_i$ )

$$V_{\text{ps}}(\vec{r}, \vec{r}') = \sum_{\vec{R}_n} v_{\text{ps}}^{(i)}(\vec{r} - \vec{R}_n) \hat{P}_i \quad (6)$$

over atoms at sites  $\vec{R}_n$ . The superposition approximation in Eq. (6) as well as the construction of  $v_{\text{ps}}^{(i)}(r)$  as approximately energy independent are *controlled* approximations: They can be tested and verified *a posteriori* in the quantitative manner.<sup>55, 56</sup>

To construct  $v_{\text{ps}}^{(i)}(r)$  we specialize the all-electron (Eq. 4) and pseudopotential [Eq. (5)] single-particle equations to atoms:

$$\left\{ -\frac{1}{2}\nabla_r^2 - (Z_c + Z_v)/r + l(l+1)/2r^2 + v_{\text{ee}}[\rho_c(r) + \rho_v(r)] + v_x[\rho_c(r) + \rho_v(r)] + v_{\text{cr}}[\rho_c(r) + \rho_v(r)] \right\} \psi_{nl}(r) = \epsilon_{nl} \psi_{nl}(r) \quad (7)$$

and

$$\left\{ -\frac{1}{2}\nabla_r^2 + v_{\text{ps}}^{(i)}(r) \hat{P}_i + l(l+1)/2r^2 + v_{\text{ee}}[n(r)] + v_x[n(r)] + v_{\text{cr}}[n(r)] \right\} \chi_{nl}(r) = \bar{\epsilon}_{nl} \chi_{nl}(r), \quad (8)$$

where  $v_{\text{ee}}$ ,  $v_x$ , and  $v_{\text{cr}}$  denote *atomic* screening potentials and  $\nabla_r^2$  is the radial Laplacian. We now seek to solve Eqs. (7) and (8) for the unknown pseudopotentials  $v_{\text{ps}}^{(i)}(r)$ , subject to a number of physically motivated constraints. In contrast to the empirical pseudopotential method,<sup>33</sup>  $v_{\text{ps}}^{(i)}(r)$  in Eq. (8) is not determined by fitting the energies  $\bar{\epsilon}_{nl}$  to experiment, leaving the wave function  $\chi_{nl}$  to be implicitly and arbitrarily fixed by such a process. Instead, we first construct physically desirable pseudo-wave-functions  $\chi_{nl}$  and then solve for the pseudopotential  $v_{\text{ps}}^{(i)}(r)$  that will produce these wave functions together with the theoretically correct orbital energies  $\bar{\epsilon}_{nl} = \epsilon_{nl}$  from the single-particle equation (8).

We first require that the pseudo-wave-function  $\chi_{nl}(r)$  be given as a linear combination of the "true" all-electron core and valence orbitals of Eq. (7):

$$\chi_{nl}(r) = \sum_{n'} C_{n, n'}^{(i)} \psi_{n', l}^{c, v}(r). \quad (9)$$

Since the pseudo-wave-functions  $\{\chi_{nl}(r)\}$  are now the lowest solutions to the (Hermitian) pseudo-Hamiltonian [Eq. (8)], they will be nodeless for each of the lowest angular symmetries. The coefficients  $\{C_{n, n'}^{(i)}\}$  will be chosen below to satisfy this condition. In a single-determinant representation, the mixing of rows and columns as given in Eq. (9) leaves the energy invariant. We then require that the orbital energies  $\bar{\epsilon}_{nl}$  of the pseudo-potential problem equal the "true" valence orbital energies  $\epsilon_{nl}$  of Eq. (7). The first condition [Eq. (9)] assures us that the pseudo-wave-functions are contained in the same core-plus-valence orbital space defined by the underlying density-functional theory; the second ( $\bar{\epsilon}_{nl} = \epsilon_{nl}$ ) ensures that the spectral properties derived from the pseudopotential single-particle equation match those of the valence electrons as described in the all-electron problem.

Without specifying at this stage the choice of the unitary rotation coefficients  $\{C_{n, n'}^{(i)}\}$ , Eqs. (7)-(9) can be solved to obtain the atomic pseudopotential  $v_{\text{ps}}^{(i)}(r)$  in terms of  $\{C_{n, n'}^{(i)}\}$  and the known quantities defining the all-electron atomic Eq. (7):

$$v_{ps}^{(i)}(r) = \left( U_i(r) - \frac{Z_v}{r} \right) + \left( -\frac{Z_c}{r} + v_{ee}[\rho_c] + v_x[\rho_c] + v_{\alpha}[\rho_c] \right) + \left( v_x[\rho_c + \rho_v] - v_x[\rho_c] - v_x[\rho_v] \right) \\ + \left( v_{\alpha}[\rho_c + \rho_v] - v_{\alpha}[\rho_c] - v_{\alpha}[\rho_v] \right) + \left( v_{ee}[\rho_c] - v_{ee}[n] \right) + \left( v_x[\rho_v] - v_x[n] \right) + \left( v_{\alpha}[\rho_v] - v_{\alpha}[n] \right), \quad (10)$$

where the "Pauli potential"  $U_i(r)$  is given by

$$U_i(r) = \frac{\sum_{n'} C_{n,n'}^{(i)} (\epsilon_{n'} - \epsilon_{n'}) \psi_{n'}(r)}{\sum_{n'} C_{n,n'}^{(i)} \psi_{n'}(r)}, \quad (11)$$

and the core, valence, and pseudocharge densities are given as

$$\rho_c(r) = \sum_{n'}^c |\psi_{n'}^c(r)|^2, \\ \rho_v(r) = \sum_{n'}^v |\psi_{n'}^v(r)|^2, \quad (12) \\ n(r) = \sum_{n'}^v |\chi_{n'}(r)|^2.$$

The atomic pseudopotential in Eq. (10) has a simple physical interpretation. The "Pauli potential"  $U_i(r)$  is the only term in  $v_{ps}^{(i)}(r)$  that depends on the wave function it operates on (i.e., "nonlocal"), whereas all other terms in Eq. (10) are common to all angular momenta (i.e., "local"). For atomic valence orbitals that lack a matching  $l$  component in the core, the all-electron valence orbitals  $\psi_{n'}^v(r)$  are nodeless, hence  $\chi_{n'} = \psi_{n'}^v$  and, from Eq. (11),  $U_i(r) = 0$  for such states. In these cases, the pseudopotential is local and purely attractive due to the dominance of the all-electron term,  $-(Z_c + Z_v)/r$ . In all other cases,  $U_i(r)$  is positive and strongly repulsive, but confined to the atomic-core region.  $U_i(r)$  replaces the core-valence orthogonality constraint and is a realization in coordinate space of Pauli's exclusion principle. Its precise form depends on the choice of the mixing coefficients  $\{C_{n,n'}^{(i)}\}$  and is discussed below. We see that the pseudopotential nonlocality, often neglected in the empirical pseudopotential approach emerges naturally in this formulation from the quantum shell structure of the atom. Similarly, Phillips's pseudopotential kinetic-energy cancellation theorem<sup>60</sup> is simply represented as a cancellation (or over-cancellation) between the nonclassical repulsive Pauli potential and the core-valence Coulomb attraction  $-Z_v/r$  [Eq. (10)].

The second term in Eq. (10) represents the total screened potential set up by the core charge density  $\rho_c(r)$ . It approaches  $-Z_c/r$  at small distances and decays to zero exponentially at the core radius (with a characteristic core screening length) due to rapid screening of the core point charge  $Z_c$  by the core electrons. The third and fourth terms in Eq. (10) represent the nonlinearity

of the exchange and correlation potentials, respectively, with respect to the interference of  $\rho_c$  and  $\rho_v$ . They measure the core-valence interactions in the system and are proportional to the penetrability of the core by the valence electrons.

The fifth term in Eq. (10) is the Coulomb orthogonality hole potential. It has its origin in the charge fluctuation  $\Delta(r) = \rho_v(r) - n(r)$  that results from the removal of the nodes in the pseudo-wavefunctions [i.e., the transformation in Eq. (9)]. The electrostatic Poisson potential set up by  $\Delta(r)$  is then given by the fifth term in Eq. (10). Finally, the last two terms in Eq. (10) represent, respectively, the exchange and correlation potentials set up by this orthogonality hole charge density  $\Delta(r)$ .

The form of the first-principles pseudopotential in Eqs. (10) and (11) makes it easy to establish contact with the successfully simplified early empirical pseudopotentials. Hence, for example, in the Abarenkov-Heine<sup>61</sup> model potential it was implicitly assumed that a pseudopotential cancellation between a repulsive Pauli force and an attractive Coulomb potential  $-Z_v/r$  exists, but instead of calculating this cancellation, its net result was assumed to take the form of a constant  $v_{ps}^{(i)}(r) = A_i$  for  $r$  smaller than some model radius  $R_i$  (inside the core), with  $v_{ps}^{(i)}(r) = -Z_v/r$  for  $r > R_i$ . Abarenkov and Heine's empirical constants  $A_i$  may be identified in the present formulation with the volume integral of  $[U_i(r) - Z_v/r]$  from the origin to  $R_i$  (neglecting all but the first term in Eq. 9). Similarly, Ashcroft<sup>62</sup> has suggested an empirical "empty-core" pseudopotential, postulating that the net result of the cancellation between  $U_i(r)$  and  $-Z_v/r$  inside the core region is zero. Indeed, for a sufficiently large core radius (i.e., of the order of Pauling's ionic radius), such a simple model well represents  $v_{ps}^{(i)}(r)$  in Eq. (10).

Up to this point, we have not yet specified the form of the transformation coefficients in Eq. (9) determining the precise relationship between the pseudo- and true wave functions. Clearly, one would like to constrain the pseudo-wave-function in Eq. (9) to be normalized. In addition, the relaxation of the orthogonality constraint may be exploited to construct  $\chi_{n'}(r)$  as nodeless for each of the lowest angular states, permitting thereby a convenient expansion of the pseudo-wave-functions in spatially simple and smooth basis functions. Even so,  $\chi_{n'}(r)$  is underdetermined: There are an infinite number of choices of  $\{C_{n,n'}^{(i)}\}$  leading

to normalized and nodeless  $\chi_{ni}(r)$ . This is a manifestation of the well-known pseudopotential nonuniqueness. The resolution of this nonuniqueness is precisely the point at which one applies one's physical intuition (and physical prejudices). Note, however, that in the present approach, any of the infinite and legitimate choices of  $\{C_{n,n}^{(i)}\}$  permits a rigorous digression from the pseudo-wave-function to the true valence wave function: the choice of a *linear* form for  $\chi_j(r)$  Eq. (9) allows for  $v_{ps}^{(i)}(r)$  to be computed from an arbitrary set  $\{C_{n,n}^{(i)}\}$  and for the resulting pseudopotential in Eq. (10) to be used to greatly simplify the calculation of the electronic structure of arbitrary molecules or solids [Eqs. (5) and (6)]. Upon completion, one can simply recover the true wave function through a core orthogonalization:

$$\psi_j(\vec{r}) = \frac{1}{N} \left( \chi_j(\vec{r}) - \sum_i^{\text{core}} \langle \chi_i | \psi_i^c \rangle \psi_i^c(r) \right), \quad (13)$$

given the known core states  $\psi_i^c(r)$ . This property is not shared by other pseudopotentials<sup>63,64,59</sup> which are modifications of the density-functional pseudopotential scheme.<sup>52-58</sup> The choice of the transformation  $\{C_{n,n}^{(i)}\}$  has, however, a direct bearing on the *transferability* of the atomic pseudopotentials from one system to another as well as on the degree to which the true valence wave functions can be reproduced without resort to core orthogonalization.

Our choice of wave-function transformation coefficients<sup>55,56,58</sup> is based simply on maximizing the similarity between the true and pseudo-orbitals [within the form of Eq. (9)] with a minimum core amplitude, subject to the constraints that  $\chi_{ni}(r)$  be normalized and nodeless. This simple choice produces highly energy-independent, and thus transferable, pseudopotentials. At the same time, the imposed wave-function similarity leads to pseudo-wave-functions that retain the full chemical information contained in the valence region of the true wave functions. Details of the numerical procedure used to obtain  $\{C_{n,n}^{(i)}\}$ , as well as numerical tests demonstrating the extremely low energy dependence of the associated pseudopotentials, are given elsewhere.<sup>56,58</sup>

The general small- $r$  expansion of the pseudo-orbital can be written as:

$$\lim_{r \rightarrow 0} \chi_{ni}(r) = A_0 r^{\eta+1} + A_1 r^{\eta+1+1} + A_2 r^{\eta+1+2}. \quad (14)$$

The choice of  $\eta \geq 2$  leads to a minimum core-amplitude pseudo-wave-function with its attendant maximum similarity to the true valence wave function. Inserting (14) into (11) and (10) leads, for any  $\eta \geq 2$ , to

$$\lim_{r \rightarrow 0} v_{ps}^{(i)}(r) = \frac{\tilde{B}_i}{r^2} - \frac{Z_v}{r} + \dots \quad (15)$$

Hence, the Simons-Bloch<sup>39,40</sup> empirical pseudo-potential [Eq. (2)] is recovered as the small- $r$  limit of the first-principles pseudopotential. We hence see that the imposition of a maximum wave-function similarity condition within the orbital subspace spanned in Eq. (9) leads to a repulsive and short-ranged Pauli potential  $U_i(r)$ . Combining such a positive  $U_i(r)$  with the negative core-attraction term  $-Z_v/r$  in Eq. (10) leads necessarily to characteristic crossing point  $v_{ps}^{(i)}(r_i^0) = 0$  at  $r = r_i^0$ . On the other hand, the choice  $\eta = 0$  leads to a soft-core pseudopotential [ $\lim_{r \rightarrow 0} v_{ps}^{(i)}(r) = \text{const}$ ]. The associated pseudo-wave-function is now finite at the origin, leading necessarily to a reduced similarity between the true and pseudo-wave-functions in the chemically relevant valence region. In general, no crossing point  $r_i^0$  occur at this limit. Our choice of the wave-function transformation in Eq. (9) produces, therefore, unique pseudopotentials by going to the extreme limit of wave-function similarity that is possible within the underlying density-functional orbital space.

Other possibilities for choosing pseudo-wave-functions exist and are discussed elsewhere.<sup>56,58,63,64</sup> These procedures involve various ways of constructing pseudo-wave-functions including components lying *outside the density-functional orbital space* [unlike Eq. (9)] and do not maintain physically transparent analytical forms such as in Eqs. (10) and (11). Hence, to distinguish them from the present density-functional pseudopotentials, we refer to these as "trans-density-functional" (TDF) pseudopotentials.<sup>56</sup> We restrict ourselves in what follows to the conceptually simpler density-functional pseudopotentials.

The approach described above for constructing orbital-dependent pseudopotentials can easily be extended to spin- and orbital-dependent potentials.<sup>65</sup> This generalization is simple, and we will not describe the details here.

Figure 1 depicts various components of the  $l=0$  atomic pseudopotential in Eq. (10) for Sb. The curve labeled (1) is the Pauli term  $U_i(r)$ , the curve labeled (2) shows the Coulomb attraction  $-Z_v/r$ , and curve (3) represents screening (terms 2-6 in Eq. 10). Finally, curve (4) shows the total pseudopotential. First-principles atomic pseudopotentials were generated for 70 atoms with  $2 \leq Z \leq 57$  and  $72 \leq Z \leq 86$  (i.e., the first five rows).

A notable feature of these potentials is the occurrence of a crossing point  $v_{ps}^{(i)}(r_i^0) = 0$  at  $r = r_i^0$ . From Eqs. (10) and (11), it is seen that, physically, this point is where the repulsive Pauli potential is balanced by the Coulomb attraction  $-Z_v/r$ , renormalized by the screened core potential, exchange-correlation nonlinearity, and the

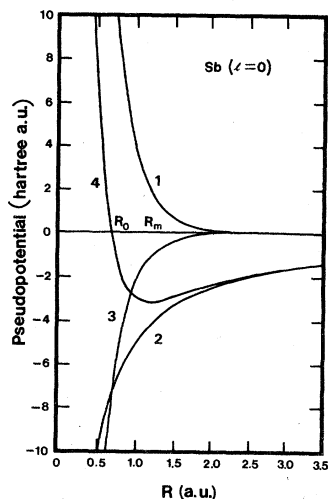


FIG. 1. Components of the atomic pseudopotential  $v_{ps}^{(l)}(r)$  [Eq. (10)] for  $l=0$  of the Sb atom: (1) Pauli potential  $U_l(r)$ , (2) the Coulomb attraction  $-Z_v/r$ , (3) core screening, and (4) the total pseudopotential.  $R_0$  and  $R_m$  denote the points of crossing and minimum, respectively.

Coulomb and exchange-correlation orthogonality hole potentials.

It seems somewhat puzzling at first sight that pseudopotentials of free-electron-like metals such as Na, Al, and K may have large momentum components or even a hard core, because the nearly-free-electron (NFE) model seems to have worked so well for these materials. However, the successes of the NFE model may have been overstated, in view of the fact that *wave-function-related properties* of the free-electron metals, such as the shape of the optical conductivity,<sup>66</sup> the metallic ground-state charge density and form factors<sup>67</sup> (compare, however, with the nonlocal pseudopotential calculations of Refs. 68 and 69), as well as the properties of impurities in metals,<sup>70</sup> are poorly reproduced by local and weak pseudopotentials. Moreover, the occurrence of rather complex crystal structures involving "simple" free-electron atoms (semimetals such as the B32 structure of LiAl, Laves phase materials such as  $K_2Cs$ , the existence of the compound  $Na_2K$ , but not  $NaK$  or  $NaK_7$ , etc.), as well as the existence of stable multiple valencies of these systems (e.g., AlF vs  $AlF_3$ , etc.) cannot be understood in terms of local NFE pseudopotentials. Hence, although such weak and NFE pseudopotentials had to be assumed for many elements (including even groups IIIA-VIA atoms) for the very popular low-order perturbation theories to be valid, the underlying assumption—that the complex chemistry of the related compounds could be understood in terms of weak and isotropic perturbations of a homogeneous electron gas—

seems naive.

Using the calculated atomic pseudopotentials of Eqs. (10)–(12), we now define the crossing points using the ground-state *screened* atomic pseudopotentials  $v_{eff}^{(l)}(r)$ :

$$v_{eff}^{(l)}(r) = v_{ps}^{(l)}(r) + \frac{l(l+1)}{2r^2} + v_{ee}[n] + v_x[n] + v_{ex}[n] \quad (16)$$

as

$$v_{eff}^{(l)}(r_i) = 0.$$

Here  $v_{eff}^{(l)}(r)$  is the total effective potential experienced in a ground-state pseudoatom by electrons with angular momentum  $l$ . These form the structural indices  $\{r_i\}$ , which we use in connection with predicting the stable crystal structure of compounds. Table I gives the  $\{r_i\}$  values of the 70 elements for which the density-functional pseudopotential equations have been solved. We have not included the heavier elements since the present pseudopotential theory is nonrelativistic. In what follows, we will hence not discuss the structural stability of lanthanide and actinide compounds.

In developing the density-functional pseudopotentials, we have tacitly assumed a specific partitioning of the atomic orbitals into core and valence. In the present theory, core orbitals are those appearing as closed-shell states in the rare-gas atom of the preceding row in the Periodic Table. Note, however, that although we may understand the low-energy electronic excitation spectra of a compound such as ZnSe by assuming that the Zn 3d orbitals belong to a passive core, such an assumption may be invalid in intermetallic compounds, where the Zn 3d orbitals can be in near resonance with the d orbitals of another element. Given the fact that any such delineation into core and valence is merely based on an arbitrary assumption on the passivity of certain orbitals to chemical interactions of interest, one may ask whether structurally meaningful orbital radii can be extracted from a pseudopotential scheme.

In fact, the choice of the orbital radii from the *screened* pseudopotential [Eq. (16)], rather than from the *bare* pseudopotential  $v_{ps}^{(l)}(r)$  in Eq. (10) (e.g., Refs. 39, 40, 48, and 49), is based precisely on an attempt to avoid such a nonuniqueness. Although the bare pseudopotential of Eq. (10) has the form

$$v_{ps}^{(l)}(r) = U_l(r) + f(Z_c, Z_v, \rho_c, \rho_v, n), \quad (17)$$

the *screened* pseudopotential can be written as

$$V_{eff}^{(l)}(r) = U_l(r) + g(Z, \rho_c + \rho_v). \quad (18)$$

Note that whereas  $U_l(r)$  [Eq. (11)] depends only

TABLE I. Classical crossing points of the self-consistently screened nonlocal atomic pseudopotentials (including the centrifugal term), in a.u. The core shell is defined in each case as the rare-gas configuration of the preceding row. The Kohn and Sham exchange is used.

Atom	$r_s$	$r_p$	$r_d$	Atom	$r_s$	$r_p$	$r_d$
Li	0.985	0.625		Sr	1.42	1.79	0.633
Be	0.64	0.44		Y	1.32	1.62	0.58
B	0.48	0.315		Zr	1.265	1.56	0.54
C	0.39	0.25		Nb	1.23	1.53	0.51
N	0.33	0.21		Mo	1.22	1.50	0.49
O	0.285	0.18		Tc	1.16	1.49	0.455
F	0.25	0.155		Ru	1.145	1.46	0.45
Ne	0.22	0.14		Rh	1.11	1.41	0.42
Na	1.10	1.55		Pd	1.08	1.37	0.40
Mg	0.90	1.13		Ag	1.045	1.33	0.385
Al	0.77	0.905		Cd	0.985	1.23	0.37
Si	0.68	0.74		In	0.94	1.11	0.36
P	0.60	0.64		Sn	0.88	1.00	0.345
S	0.54	0.56		Sb	0.83	0.935	0.335
Cl	0.50	0.51		Te	0.79	0.88	0.325
Ar	0.46	0.46		I	0.755	0.83	0.315
K	1.54	2.15	0.37	Xe	0.75	0.81	0.305
Ca	1.32	1.68	0.34	Cs	1.71	2.60	
Sc	1.22	1.53	0.31	Ba	1.515	1.887	0.94
Ti	1.15	1.43	0.28	La	1.375	1.705	0.874
V	1.09	1.34	0.26	Hf	1.30	1.61	0.63
Cr	1.07	1.37	0.25	Ta	1.25	1.54	0.605
Mn	0.99	1.23	0.23	W	1.22	1.515	0.59
Fe	0.95	1.16	0.22	Re	1.19	1.49	0.565
Co	0.92	1.10	0.21	Os	1.17	1.48	0.543
Ni	0.96	1.22	0.195	Ir	1.16	1.468	0.526
Cu	0.88	1.16	0.185	Pt	1.24	1.46	0.51
Zn	0.82	1.06	0.175	Au	1.21	1.45	0.488
Ga	0.76	0.935	0.17	Hg	1.07	1.34	0.475
Ge	0.72	0.84	0.16	Tl	1.015	1.22	0.463
As	0.67	0.745	0.155	Pb	0.96	1.13	0.45
Se	0.615	0.67	0.15	Bi	0.92	1.077	0.438
Br	0.58	0.62	0.143	Po	0.88	1.02	0.425
Kr	0.56	0.60	0.138	At	0.85	0.98	0.475
Rb	1.67	2.43	0.71	Rn	0.84	0.94	0.405

on orbitals with angular momentum  $l$ , the valence pseudo-charge-density  $n(r)$  [Eq. (12)] depends on all orbitals that are assigned as valence states. Consequently, for example, if the Zn  $3d$  orbitals are assumed to be a part of the core, the *bare* pseudopotential  $v_{ps}^{(1)}(r)$  for  $s$  and  $p$  electrons is different than if the  $d$  electrons were assigned to the valence. In contrast, it follows from Eq. (18) that the *screened* pseudopotential  $v_{\text{eff}}^{(1)}(r)$  for  $l=0,1$  is invariant under such a change in the assignment of the  $d$  electrons. Our definition of the structural indices  $r_l$  is therefore independent of the assignment of orbitals  $\psi'_{nl}(r)$  from *other* angular shells as core or valence. Also note that the definition of orbital radii from the screened pseudopotentials of Eq. (16) permits a direct inclusion of electronic exchange and correlation effects in the structural coordinates  $r_l$  (see Ref. 71), whereas the semi-

classical electron concentration factor<sup>6</sup> is represented simply by  $Z_v$ .

#### B. Simple universal form the density-functional pseudopotentials

The idea of atomic radii is not new in pseudopotential theory (see Sec. II). The basic thrust of the pseudopotential concept is to transform the chemical picture of the existence of an *orbital subspace* of nearly chemically inert core states into a delineation either in *configuration space* or in *momentum space* of a core region of the potential (with its attendant cancellation effects between orthogonality repulsion and Coulomb attraction) and a valence region (with its weaker effective potential). What is new in the present approach is that whereas in the empirical pseudopotential

methods the radii were imposed extraneously, either explicitly<sup>40,61,62,72,73</sup> or implicitly,<sup>31,33</sup> the present theory provides them as a natural fingerprint of the internal quantum structure of the free atom. In the empirical approach, the radii are in turn transferred from various sources (Pauling ionic radii, fitting energy eigenvalues to atomic term values, optical reflectivity of semiconductors, or the Fermi surface of metals, etc.), such that although a desired fit to selected experimental observables is achieved, the underlying electronic and structural regularities may be obscured by fitting to different physical properties or by postulating certain arbitrary analytic forms for  $v_{ps}^{(i)}(r)$ .

Given that the analytic form of the pseudopotential in the present approach is not assumed but rather emerges as a consequence of requiring a maximum similarity between the all-electron and pseudo-wave-functions in the tail region, it however is possible to deduce *a posteriori* a universal analytic form through a fitting procedure. Such a fit can be done in two different ways: either emphasizing a high numerical accuracy for the fit (and hence using rather complicated or many fitting functions) or by using a physically transparent fitting function, sacrificing to some extent the numerical accuracy but obtaining the correct *regularities* of the pseudopotentials. This has been attempted by Lam *et al.*<sup>74</sup> using the simple form:

$$v_{ps}^{(i)}(r) \approx \frac{C_{1i}}{r^2} e^{-c_{2i}r} - \frac{Z_c}{r} e^{-c_{3i}r} - \frac{Z_v}{r}. \quad (19)$$

The coefficients  $\{C_{1i}, C_{2i}, \text{ and } C_{3i}\}$  are tabulated by Lam *et al.* Although more complicated forms than Eq. (19) have also been used,<sup>74</sup> Eq. (19) reveals a very important characteristic of the density functional pseudopotentials: To within a reasonable approximation, the constants  $C_{1i}, C_{2i}, \text{ and } C_{3i}$  are linear functions of the atomic number, i.e.,

$$C_{1i} \approx a_i + b_i Z, \quad C_{2i} \approx c_i + d_i Z, \quad C_{3i} \approx e + f Z. \quad (20)$$

This constitutes a significant reduction in the number of degrees of freedom required to specify the potential and reveals the regularities of the Periodic Table through the coordinates  $(Z_c, Z_v)$ . This can be contrasted with the empirical pseudopotential approach in which such regularities are often obscured by fitting certain atomic pseudopotentials to optical data,<sup>31</sup> whereas others are fit to metallic Fermi-surface data and the resistivity of metals<sup>75</sup> or to atomic term values.<sup>39,61,76</sup>

The existence of a simple linear scaling relationship in Eqs. (19) and (20) establishes a mapping of Mendeleev's classical dual coordinates  $Z_c$  and  $Z_v$  characterizing the digital structure of the periodic table, into a more refined quantum-mechan-

ical coordinate system,  $r_s(Z_c, Z_v)$ ,  $r_p(Z_c, Z_v)$ , and  $r_d(Z_c, Z_v)$ . Given the fact that Mendeleev's dual coordinates  $(Z_c, Z_v)$  are already suggestive of broad structural trends (e.g., the AB compounds with  $Z_v^A=3, Z_v^B=5$  tend to form zinc-blende structures for large  $Z_c^{A,B}$  values, while compounds with  $Z_v^A=1, Z_v^B=7$  tends to form rocksalt structures, etc.), it is only reasonable to expect that with their present resolution into *anisotropic* orbital components, far more sensitive structural coordinates can be achieved.

The density-functional atomic pseudopotentials have been previously used for self-consistent electronic-structure calculations. These include applications to diatomic molecules [ $O_2$  (Ref. 77),  $Si_2$  (Ref. 78)], tetrahedrally bonded semiconductors such as Si (Refs. 58 and 79), Ge (Ref. 58), and GaAs (Ref. 80), elemental transition-metal solids Mo (Refs. 81 and 82) and W (Ref. 82), the relaxed GaAs (110) surface (Ref. 80), as well as to the prediction of the cohesive energies, bulk moduli and equilibrium lattice constant of Si (Ref. 83), Mo, and W (Ref. 82). Very good agreement is obtained with the available experimental data pertaining to ground-state properties.

#### IV. TRENDS IN ORBITAL RADII

##### A. Chemical regularities

We have argued that the classical turning points  $r_t$  of the screened density-functional *atomic* pseudopotentials form a useful elemental distance scale for *solids*. One may then ask if indeed such atomic quantities retain their significance in the solid state. To answer this, we have performed a self-consistent band-structure calculation for bcc tungsten using our atomic pseudopotentials. This is done by assuming that the crystalline pseudopotential  $V_{ps}^{(i)}(\vec{r})$  is a superposition of the atomic pseudopotentials  $v_{ps}^{(i)}(r)$  [Eq. (6)], but the screening  $V_{scr}^v[n]$  is calculated from the self-consistent Bloch wave functions of the solid<sup>82</sup> (rather than from atomic orbitals). The resulting band structure, Fermi surface, and optical spectra are in very good agreement with previously published results. One can now use the self-consistent crystalline charge density  $n(\vec{r})$ , calculate the Coulomb, exchange, and correlation screening in the solid, and extract from that the screened *solid-state* pseudopotentials  $V_{off}^{(i)}(\vec{r})$  [Eq. (1)] and their classical turning points. Obviously, such a solid-state screened potential has a different form in the different crystalline directions  $[h, k, l]$ , resulting in spatially anisotropic orbital radii  $r_i[h, k, l]$ . Figure 2 shows the crystalline tungsten pseudopotential (dashed lines) as well as the three components of the screening (evaluated with respect to the

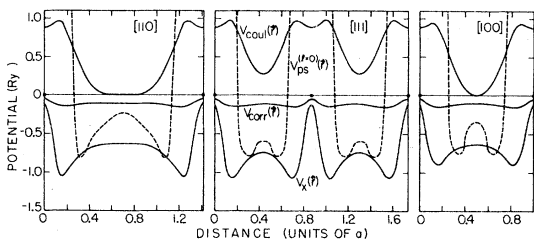


FIG. 2. Self-consistent screening potential [interelectronic Coulomb  $V_{\text{coul}}(\mathbf{r})$ , exchange  $V_x(\mathbf{r})$ , and correlation  $V_{\text{corr}}(\mathbf{r})$ ] and pseudopotential  $v_{\text{ps}}^{(l=0)}(\mathbf{r})$  for bcc tungsten in different directions in the crystal.

Fermi energy) in the solid. Although the screened pseudopotentials show a pronounced directional character, the solid-state radii, lying in the core region of the atoms, show only a small directional anisotropy:  $r_0[111] = 1.279 \pm 0.002$  a.u.,  $r_0[001] = 1.214 \pm 0.002$  a.u., and  $r_0[110] = 1.256 \pm 0.002$  a.u., compared with the isotropic atomic value  $r_0 = 1.225$  a.u. and the average crystalline value of 1.25 a.u. The near invariance of these radii with respect to the chemical environment should be contrasted with the pronounced dependence of the classical crystallographic radii<sup>84</sup> on chemical factors (coordination number, valency, spin state, etc.).

Inspection of the atomic pseudopotentials immediately reveals some clear regularities. This may be appreciated from Fig. 3, which shows the radius  $r_0^{\text{min}}$  at which the  $l=0$  pseudopotential has its minimum, plotted against the depth of the minimum  $W_0$ . The column structure of the Periodic Table is immediately apparent. At the upper left corner of the figure, we see elements such as Cs and Rb, characterized by a very shal-

low and extended pseudopotential; these elements are indeed the least electronegative in the first five rows of the Periodic Table. In the lower right corner, we find elements such as F and O, which are characterized by very deep and localized pseudopotentials; these are indeed the most electronegative elements. Clearly, as the electronegativity is a measure of the power of an atom to gain extra electrons from its environment and at the same time keep its own electrons, such a propensity is reflected in the potential-well structure of  $v_{\text{ps}}^{(l)}(r)$ . In contrast with the thermochemical or dielectric electronegativity scales, however, the present orbital radii define an *anisotropic* (or  $l$ -dependent) electronegativity scale.

We see in Fig. 3 that the first-row elements are somewhat separated from the other elements, the former having deeper potentials than might have been expected from extrapolating the data for other rows. This phenomenon, resulting from a weak pseudopotential kinetic-energy cancellation for the first-row elements, is also clearly reflected in the thermochemical stability of the corresponding compounds. As we move from the right to the left of the Periodic Table, one sees in Fig. 3 that the elements belonging to a given column can be well characterized by their potential radii alone, the potential depth being nearly constant. This seems to be the basis for the success of the empty-core pseudopotentials<sup>62</sup> postulated for simple metals, in which  $v_{\text{ps}}(r)$  is assumed to be zero within a sphere of radius  $R_{\text{ec}}$ . In this approach only the variation in  $R_{\text{ec}}$  within a column in the Periodic Table was used to characterize a large variety of transport and structural data for the corresponding metals.<sup>62,75</sup> In fact, one finds that these empirical

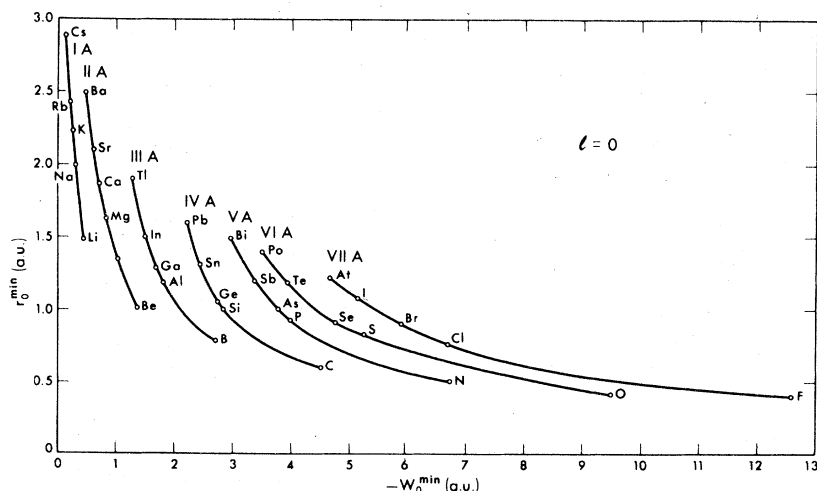


FIG. 3. The correlation between the radius  $r_0^{\text{min}}$  at which the  $s$  pseudopotential has its minimum and the depth of the minimum  $-W_0^{\text{min}}$ , for the nontransition elements.

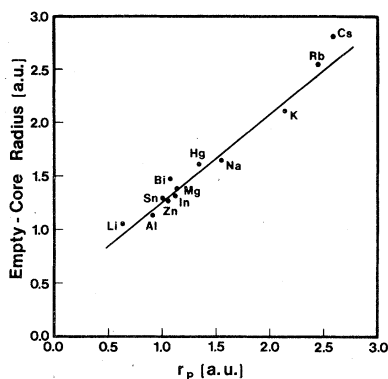


FIG. 4. Correlation between Ashcroft's empty-core pseudopotential radius and the  $p$ -orbital radius of the present density-functional screened pseudopotential (Table I).

empty-core radii used to fit resistivity data may be identified, within a linear scale factor, with the  $r_p$  screened pseudopotential coordinate (Fig. 4). Whereas the alkali elements are characterized predominantly by a single coordinate (Fig. 3), in line with their free-electron properties associated with a shallow pseudopotential, the elements to their right are characterized by a dual-coordinate system. The regularities in these dual coordinates also reflect well-known chemical trends: For example, the tendency towards metalization in the C-Si-Ge-Sn-Pb series is represented by the increased delocalization and reduced depth in their pseudopotentials, etc.

Having discussed the periodic trends exhibited by the atomic pseudopotentials, we now turn to their significance in the establishment of elementary *distance* and *energy* scales, which are quantum-mechanical extensions of similar semiclassical scales discussed in the Introduction.

Figures 5 and 6 display the multiplet-average experimental ionization energy  $E_i$  of the atoms,<sup>85</sup> plotted against the reciprocal orbital radius  $r_i^{-1}$ . For each group of elements, we show two lines:  $E_s$  vs  $r_s^{-1}$  and  $E_p$  vs  $r_p^{-1}$ . The striking result is that the theoretical  $r_i^{-1}$  is seen to form an accurate measure of the experimental orbital energies and hence can be used as an elementary orbital-dependent energy scale, much like Mulliken's electronegativity. Indeed, since  $r_i^{-1}$  is a measure of the scattering power of a screened pseudopotential core towards electrons with angular momentum  $l$ , it naturally forms an electronegativity scale. There is an interesting relation between this picture and Slater's concept of orbital electronegativity within the density-functional formalism.<sup>86</sup> In his approach, the spin-orbital electronegativity  $X_i$  is defined as the orbital energy  $\epsilon_i$  of the density-functional Hamiltonian, which in turn equals the

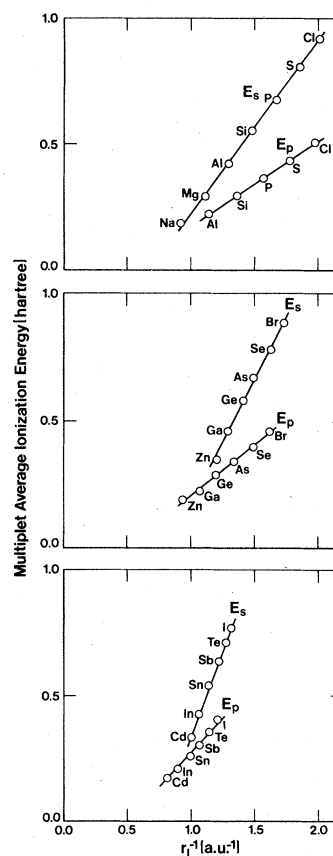


FIG. 5. Correlation between the observed  $l$ th orbital multiplet-averaged ionization energies  $E_i$  and the reciprocal orbital radius  $r_i^{-1}$  (Table I) for the polyvalent elements.

derivative of the total energy  $E$  with respect to the  $i$ th orbital occupation number:  $X_i = \epsilon_i = \partial E / \partial n_i$ . In the limit where  $E$  is a quadratic function of  $n_i$ , this orbital electronegativity reduces to Mulliken's form. This definition is based on the notion that a chemical reaction takes place when electrons will flow from the highest occupied orbitals of a reactant to the lowest unoccupied orbitals with which a

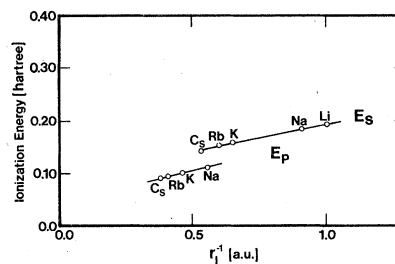


FIG. 6. Correlation between the ground-state ( $E_s$ ) and excited-state ( $E_p$ ) orbital ionization energies of the alkali atoms and the corresponding reciprocal orbital radius  $r_i^{-1}$  (Table I).

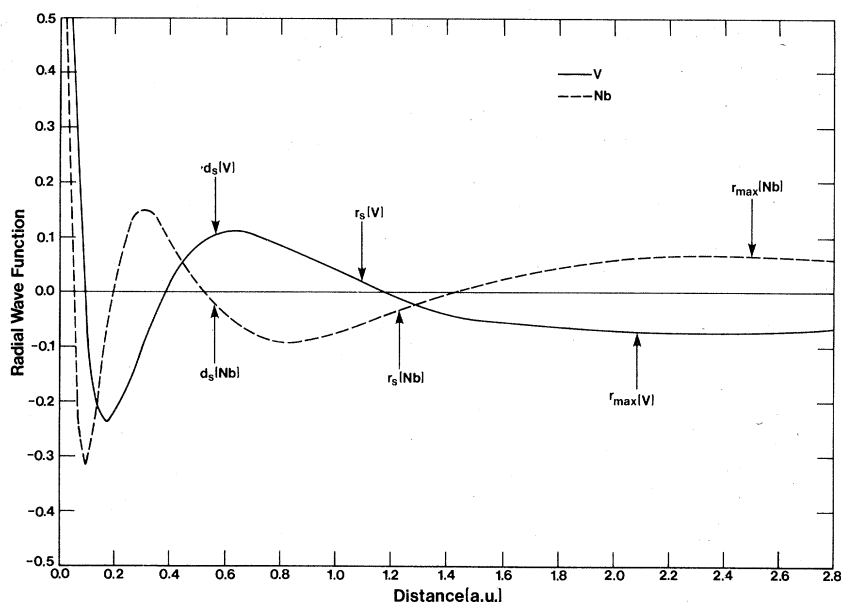


FIG. 7. Radial  $s$ -type all-electron wave functions for V and Nb.  $r_{\max}$  denotes the position of the outer orbital maxima,  $r_s$  is the screened pseudopotential radius, and  $d_s$  is the average node position. Note that  $r_s$  is pinned inwards of the last node and outwards of  $d_s$ .

finite overlap occurs. Since the present  $r_i^{-1}$  coordinate scales approximately with the orbital energy  $\epsilon_i$ , the former coordinate is a realization of Slater's electronegativity in a pseudopotential representation.

The orbital radii  $r_i$  also form an interesting distance scale.<sup>47</sup> Consider an all-electron valence atomic wave function such as the  $4s$  and  $5s$  orbitals of V and Nb, respectively, depicted in Fig. 7. These wave functions have their outer maxima at the points denoted by  $r_{\max}$  and have a number of nodes inwards to  $r_{\max}$ . An algebraic average taken

for all node positions in each wave function shows that these average positions (denoted by  $d_i$ ) are pinned at a certain distance from the pseudopotential orbital radius  $r_i$ . Figure 8 shows the average node position  $d_i$  of the outer all-electron  $s$ -type valence orbital plotted against  $r_s$ , and Fig. 9 shows similar results for  $d$  orbitals (only the first and last element of each row are denoted by the chemical symbol). We find that the orbital radius  $r_i$  scales linearly with the average node position, where the row-dependent scale factor increases monotonically with the position of the period in the table of elements (e.g., the scale equals 1.0, 1.5, 2.0, 2.3, and 2.7 for periods 1–5, respectively).

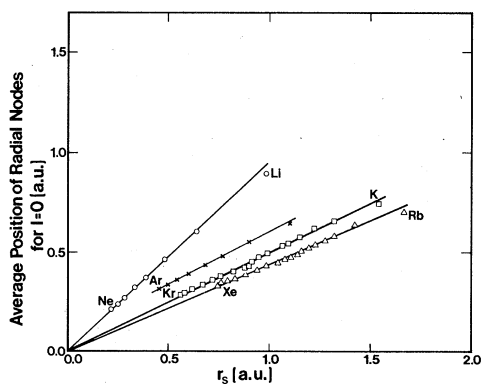


FIG. 8. Correlation between the average node position in the valence all-electron  $s$  wave function and the screened pseudopotential radius  $r_s$  (Table I). The first and last atom of each row are denoted by chemical symbols.

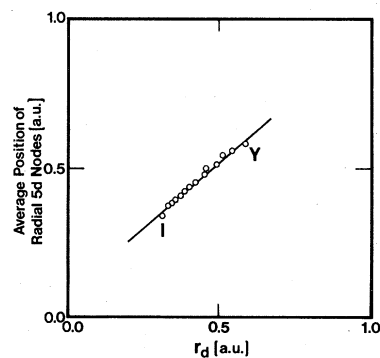


FIG. 9. Correlation between the average node position in the valence all-electron  $d$  wave function and the screened pseudopotential radius  $r_d$  (Table I) for the  $4d$  elements.

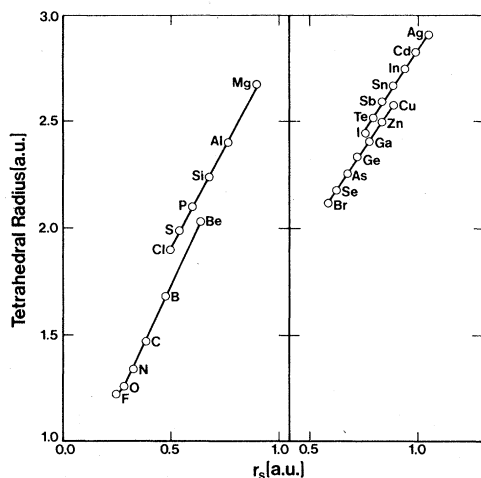


FIG. 10. Relation between Pauling's tetrahedral radius and the  $s$ -orbital radius of the screened pseudopotential (Table I).

It is seen that the orbital radii  $r_i$  form, therefore, an intrinsic length scale in that they carry over from the true wave functions the information on the average node position. Hence, the dual coordinates  $\{r_i, r_i^{-1}\}$  satisfy the semiclassical ideas underlying many successful structural factors<sup>5-7</sup> in forming elementary energy and length scales.

An additional intriguing feature of these orbital radii is their simple correlation with Pauling's tetrahedral radii.<sup>5</sup> As seen in Fig. 10, the tetrahedral radii can be identified with the  $r_s$  coordinate to within a row-dependent scale factor.

While the individual  $r_s$  and  $r_p$  radii measure the effective extent of the quantum cores of  $s$  and  $p$  symmetry, the sum  $R_\sigma^A = r_s^A + r_p^A$  provides a measure of the total size of the effective core of atom

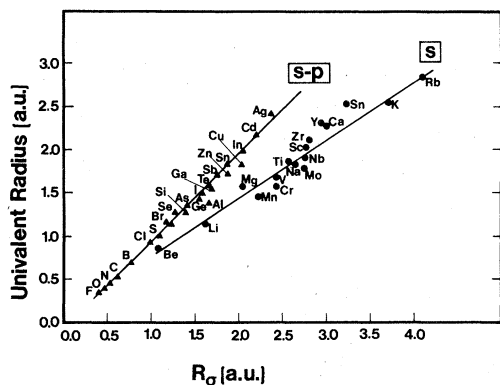


FIG. 11. Relation between Pauling's univalent radii and the total  $s$ - $p$  screened pseudopotential radius  $R_\sigma = r_p + r_s$ . Note that this  $R_\sigma$  scale separates the univalent radii into a group of predominantly  $s$ -bonding elements (full circles) and  $s$ - $p$  bonding elements (full triangles).

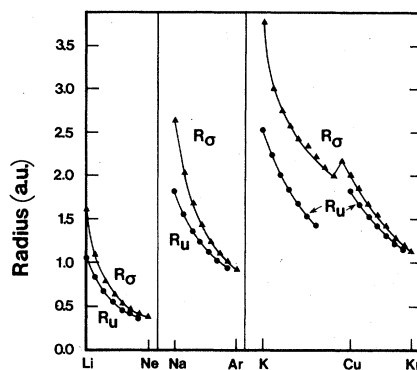


FIG. 12. Correlation between Pauling's univalent radii  $R_u$  and the total  $s$ - $p$  screened pseudopotential radius  $R_\sigma = r_s + r_p$ . Only the first and last elements in each row are denoted by the chemical symbol. Note the nonmonotonic break in  $R_u$  and  $R_\sigma$  occurring at the end of the  $3d$  transition series.

A. Figure 11 depicts  $R_\sigma^A$  versus Pauling's univalent radii for the first three periods of the table of elements, whereas Fig. 12 shows their explicit correlation. A similar correlation exists with Gordy's covalent radius.<sup>87</sup>  $R_\sigma^A$  closely follows the regularities of the univalent radii, including their discontinuity at the end of the transition elements. Examination of Fig. 11 reveals that the present  $R_\sigma^A$  coordinate provides a natural separation of Pauling's univalent radii into those that pertain to atoms sustaining  $s$ - $p$  covalently bonded compounds and those in which the  $s$  electrons largely dominate the structural properties. It is remarkable that the orbital radii derived from a pseudopotential formulation of *atomic physics* provide such a close reproduction of the length scale derived experimentally from *solid-state physics* (e.g., the empty-core radii in Fig. 4, and Pauling's tetrahedral and univalent radii in Fig. 10 and Figs. 11 and 12, respectively).

We have concentrated in this section on revealing the most significant correlations between the orbital radii and some *transferable* (rather than compound-dependent) semiclassical coordinates. We will not describe correlations with compound-dependent physical properties (e.g., melting points, deviations from ideal  $c/a$  ratio in wurtzite structures, elastic constants, etc.) not only because this may be too excessive, but also because we believe that many more such interesting correlations are likely to be discovered in the future. Such correlations between atomic  $\{r_i\}$  values and physical properties  $G_{AB}^{(1)}$ ,  $G_{AB}^{(2)}$ , etc., may not only serve to systematize those properties but could also point to the underlying dependencies between the seemingly unrelated physical observables  $G_{AB}^{(1)}$ ,  $G_{AB}^{(2)}$ , etc.

### B. Screening length and orbital radii

One can view the quantity  $r_i^{-1}$  as being an orbital-dependent screening constant pertinent to the scattering of valence electrons from an effective core. For the nontransition elements, one finds (cf. Fig. 13), as expected, that  $r_i^{-1}$  falls off monotonically with decreasing valence charge  $Z_v$ , reflecting a more effective screening. However, for the  $3d$ ,  $4d$ , and  $5d$  transition series (Fig. 14), one finds two distinct behaviors: Although  $r_d^{-1}$  is a simple, monotonic function, both  $r_s^{-1}$  and  $r_p^{-1}$  show a break at the point where the  $d$  shell is filled. This is intimately related to a similar trend in the orbital shielding constants  $Z_i^*$  calculated by Clementi and Roetti<sup>88</sup> as a rigorous extension of Slater's screening rules. As seen in Fig. 15, the reciprocal screening lengths  $(Z_i^*)^{-1}$  for the nontransition elements follow a regular monotonic trend, but those from the  $3d$  transition series (Fig. 16) show a characteristic break around Cu-Zn, much like the corresponding reciprocal radii  $r_i^{-1}$ .

This dual behavior of  $r_i^{-1}$  separates the predominantly  $d$ -screening domain of the transition elements from the  $s$ - $p$  screening domain of the post-transition elements. Note that  $r_i^{-1}$  and  $Z_i^*$  show uniquely this dual behavior, whereas most chemical and physical quantities are simple monotonic func-

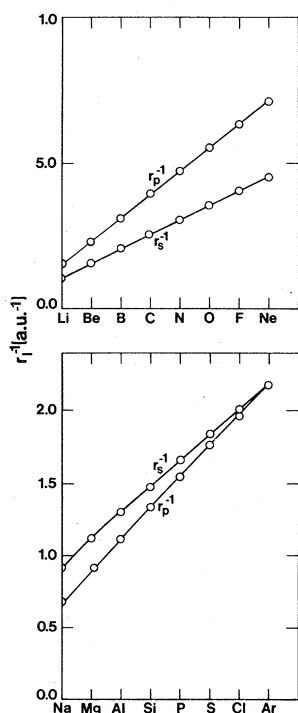


FIG. 13. Regularities in the orbital electronegativity parameters  $r_i^{-1}$  (Table I) for the elements of the first two rows.

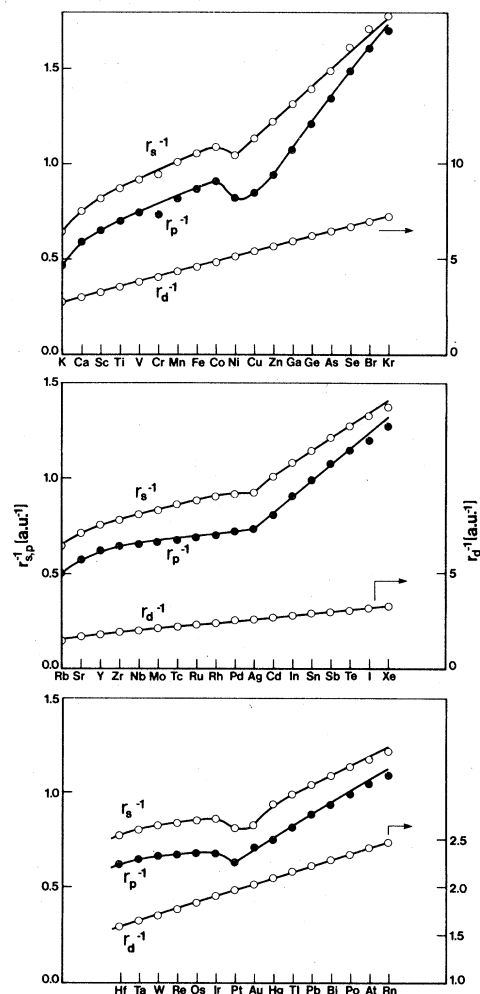


FIG. 14. Regularities in the orbital electronegativity parameters  $r_i^{-1}$  (Table I) for the  $3d$ ,  $4d$ , and  $5d$  transition series. Note the linearity of the  $r_d^{-1}$  scale compared with the break in the  $r_s^{-1}$  and  $r_p^{-1}$  scales.

tions of the atomic position in these rows. It is interesting to note that such effects are clearly manifested by  $s$  and  $p$  coordinates rather than by the  $d$  coordinate. This has a central role in the

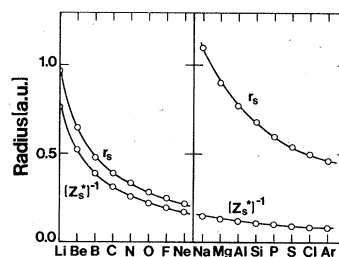


FIG. 15. The regularities in the reciprocal  $s$ -orbital shielding constants (Ref. 88)  $(Z_s^*)^{-1}$  for the nontransition elements, compared with the screened pseudopotential radii  $r_s$ .

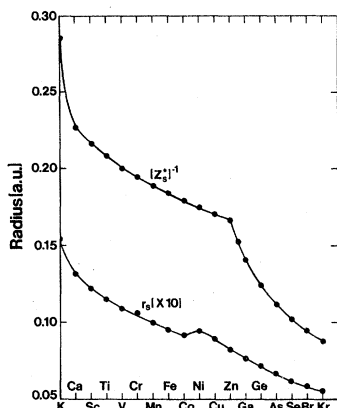


FIG. 16. Regularities in the reciprocal orbital shielding constants (Ref. 88)  $(Z_s^*)^{-1}$  for the third-row elements, compared with the screened pseudopotential radii  $r_s$ . Note the break at the end of the transition series.

structural significance of the  $s$ - $p$  coordinates even for compounds containing transition elements.

### C. Comparison with other orbital radii

Figure 17 compares the empirical stripped-ion radii of Simons and Bloch (SB) with the present theoretical values of the density-functional orbital radii for the 41 nontransition elements calculated by SB. The latter set has recently been corrected

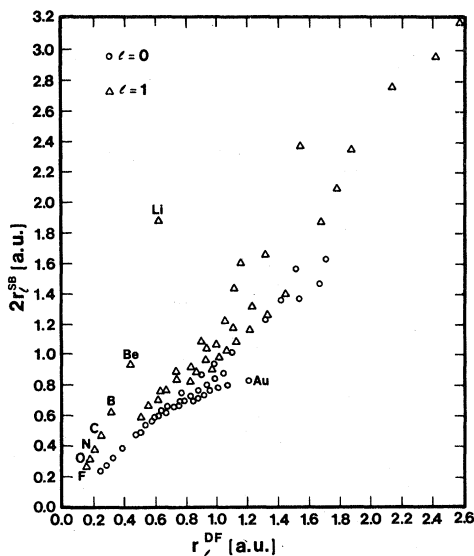


FIG. 17. Correlation between the Simons-Bloch empirical orbital radii  $r_l^{SB}$  and the present screened pseudopotential density-functional radii  $r_l^{DF}$  (Table I) for the 41 nontransition elements given by Simons and Bloch. The  $l=1$  coordinates of the first-row elements and the  $l=0$  coordinate of Au showing the largest spread are denoted by their chemical symbol.

for the post-transition elements<sup>47</sup> relative to the set used by Chelikowsky and Phillips<sup>43</sup> and Machlin, Chow, and Phillips.<sup>42</sup> Figure 17 includes the corrected values (e.g., the  $l=0$  crossing point radii for Cu, Ag, and Au are 0.38, 0.44, and 0.41 a.u., instead of 0.21, 0.22, and 0.13 a.u., respectively<sup>42,43</sup>). These large corrections change quantitatively some of the results of these previous authors in analyzing the nonoctet crystal structures, regularities of melting temperatures, as well as the decomposition of Miedema's heat-of-formation model into elemental orbital radii.

Figure 18 compares the recent orbital radii developed by Andreoni, Baldereschi, Biemont, and Phillips (ABBP; Refs. 48 and 49) with the present orbital radii, for the 27 nontransition elements calculated by ABBP. The ABBP radii are obtained from a two-parameter fit of both the Hartree-Fock stripped-ion orbital energies as well as the peak position of the orbital wave functions. The values for the eight  $3d$  transition elements given by ABBP are not included in Fig. 18 since, as indicated by these authors, and as we confirm, they are not as reliable.

It can be seen that although the empirical SB radii correlate overall with the present radii, the scatter is fairly large. In particular, the SB scheme predicts  $r_s < r_p$  for the first-row elements, whereas the present and the ABBP scheme, which attempt to reproduce both energies and wave functions, show  $r_s > r_p$ . The ABBP radii correlate well with the present radii<sup>49</sup> for the 27 nontransition

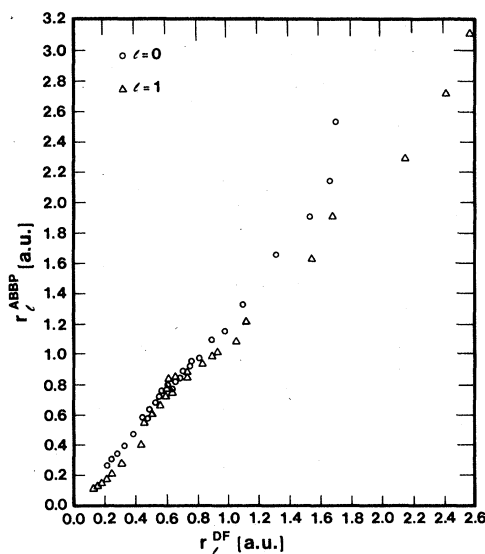


FIG. 18. Correlation between the Andreoni, Baldereschi, Biemont, and Phillips (Ref. 48) orbital radii  $r_l^{ABBP}$  and the present screened pseudopotential density-functional radii  $r_l^{DF}$  (Table I) for the 27 nontransition elements given by ABBP.

elements. Other plots (e.g., correlation of  $|r_s^A - r_p^A|$  or  $|r_s^A + r_p^A|$  between the various schemes) lead to similar conclusions.

## V. APPLICATIONS TO PREDICTION OF CRYSTAL STRUCTURE OF 565 BINARY COMPOUNDS

### A. Structural plots

The orbital radii  $\{r_i\}$  derived here can be applied to systematize the stable crystal structure of com-

pounds in the same way as discussed by St. John and Bloch,<sup>41</sup> Machlin *et al.*,<sup>42</sup> and Zunger and Cohen.<sup>54</sup> Having, however, the orbital radii of all atoms belonging to the first five rows in the Periodic Table, the present theory can be applied to a far larger data base of crystals (565) than has been attempted previously (50–80 compounds).

Our first step was to compile a list of binary *AB* compounds whose atoms belong to the first five rows of the Periodic Table. We were interested

TABLE II. *AB* crystal structures used in the structural plots. When two entries appear for the number of compounds, the first indicates the number of suboctet compounds and the second denotes the number of nontransition element superoctet compounds.

<i>Strukturberichte</i> or Pearson symbols	Space group	Unit cell	Prototype	Number of compounds
Octet				
B1	<i>Fm3m</i>	cubic	NaCl	65
B2	<i>Pm3m</i>	cubic	CsCl	3
B3	<i>F43m</i>	cubic	ZnS	29
B4	<i>P6<sub>3</sub>mc</i>	hexagonal	ZnO	11
A4	<i>Fd3m</i>	cubic	diamond	4
Total				112
Nonoctet				
B1	<i>Fm3m</i>	cubic	NaCl	33+8
B2	<i>Pm3m</i>	cubic	CsCl	122+2
B8 <sub>1</sub>	<i>P6<sub>3</sub>/mmc</i>	hexagonal	NiAs	62+3
B10	<i>P4/nmm</i>	tetragonal	PbO	0+2
B11	<i>P4/nmm</i>	tetragonal	CuTi	7
B16	<i>Pnma</i>	orthorhombic	GeS	0+7
B19	<i>Pnma</i>	orthorhombic	CuCd	11
B20	<i>P2<sub>1</sub>3</i>	cubic	FeSi	17
B27	<i>Pnma</i>	orthorhombic	FeB	16
B31	<i>Pnma</i>	orthorhombic	MnP	30
B32	<i>Fd3m</i>	cubic	NaTl	7
B33	<i>Cmcm</i>	orthorhombic	CrB	41
B35	<i>P6/mmm</i>	hexagonal	CoSn	3
B37	<i>I4/mcm</i>	tetragonal	SeTl	0+3
B <sub>h</sub>	<i>P6<sub>3</sub>m2</i>	hexagonal	MoP	4
cP64	<i>P43n</i>	cubic	KGe	6
hP24	<i>P6<sub>3</sub>/mmc</i>	hexagonal	LiO	3
L1 <sub>0</sub>	<i>P4/mmm</i>	tetragonal	CuAu	27
mC24	<i>C2/m</i>	monoclinic	AsGe	0+4
mC32	<i>C2/c</i>	monoclinic	NaSi	1
mP16	<i>P2<sub>1</sub>/c</i>	monoclinic	AsLi	4
mP32	<i>P2<sub>1</sub>/n</i>	monoclinic	NS	0+5
oC16	<i>Cmcm</i>	orthorhombic	NaHg	1
oC16	<i>Cmca</i>	orthorhombic	KO	1
oC48	<i>Cmc2<sub>1</sub></i>	orthorhombic	SiP	0+1
oI8	<i>Immm</i>	orthorhombic	RbO	4
oP16	<i>P2<sub>1</sub>2<sub>1</sub>2<sub>1</sub></i>	orthorhombic	NaP	6
tI8	<i>I4/mmm</i>	tetragonal	HgCl	0+3
tI32	<i>I4<sub>1</sub>/a</i>	tetragonal	LiGe	1
tI32	<i>I4/mcm</i>	tetragonal	TlTe	0+1
tI64	<i>I4<sub>1</sub>/acd</i>	tetragonal	NaPb	7
Total				453

in the most stable crystal form of each compound and in a structure that appears in the phase diagram at (or close to) a 50 at. %–50 at. % composition. We started the compilation by reviewing standard tables,<sup>7,12,89-95</sup> as well as a number of basic papers (e.g., Refs. 96–99), which give useful tables for particular structures. Whenever we have identified in this literature either a conflict in assigning a crystal structure or expressions of doubt as to the identification of the structure, occurrence of other structures at somewhat different pressures or temperatures, substantial deviation from 1:1 stoichiometry, etc., we have made use of a computer-assisted literature search to find the original papers for the compounds in question. In this way, we have surveyed some 180 references. We have identified from standard sources as well as from an extended computer search a total of 565 binary  $AB$  compounds that are near-stoichiometric, ordered, and formed from atoms belonging to the first five rows of the Periodic Table. Their distribution among the various crystal structures is given in Table II. The compounds included are listed in Appendix I according to their structural groups.

This data base of 565 binary compounds exhibits an enormous range of physical, structural, and chemical properties. Using the terminology of the semiclassical structural factors, one notes the large range of conductivity properties spanned by these compounds (insulators, semiconductors, semi-metals, metals, superconductors), the electronegativity difference between the constituting atoms (covalent versus highly ionic), coordination numbers (12 to 2), relative ionic sizes of the  $A$  and the  $B$  atom, bonding type (covalent, ionic, metallic, etc.), range of heats of formation ( $\approx 1$ –150 kcal/mole), electron-per-atom ratios ( $\approx 1.5$  to 8–9), etc. Given this distribution of the 112 octet compounds and 453 nonoctet compounds into 5 and 31 different crystal structures, respectively exhibiting a diverse range of properties, we now ask how well can the atomically derived orbital-radii scheme explain such a distribution.

We construct from the  $s$  and  $p$  atomic-orbital radii the dual coordinates for an  $AB$  compound as:

$$\begin{aligned} R_{\sigma}^{AB} &= |(\gamma_p^A + \gamma_s^A) - (\gamma_p^B + \gamma_s^B)|, \\ R_{\tau}^{AB} &= |\gamma_p^A - \gamma_s^A| + |\gamma_p^B - \gamma_s^B|. \end{aligned} \quad (21)$$

Here,  $R_{\sigma}^{AB}$  is a measure of the difference between the total effective core radii of atoms  $A$  and  $B$  (i.e., size mismatch), whereas  $R_{\tau}^{AB}$  measures the sum of the orbital nonlocality of the  $s$  and  $p$  electrons on each site. Using the definition (Eq. 21) and the values of the orbital radii given in Table I, we construct  $R_{\sigma}^{AB}$  vs  $R_{\tau}^{AB}$  maps for the binary com-

pounds. Such maps are shown for 112 octet compounds in Fig. 19 and for 356 of the nonoctet compounds in Fig. 20. (Since the symbols in Fig. 20 are crowded, if any two overlapped they were artificially moved to show them separately).

We identify each structure by a different symbol and search in the  $R_{\sigma}^{AB}$ - $R_{\tau}^{AB}$  plane for the smallest number of straight lines, enclosing minimal areas, best separating the different structures. In some cases, there exists a unique solution to this topological problem; in other cases (e.g.,  $B33$  and the  $cP64$  and  $tI64$  structures), there are a number of permissible solutions. However, in these cases it seems to make little difference which line is chosen. While we could have lowered the number of "misplaced" compounds by using more complex lines, we feel that the more stringent criterion of using straight lines provides us with a better chance

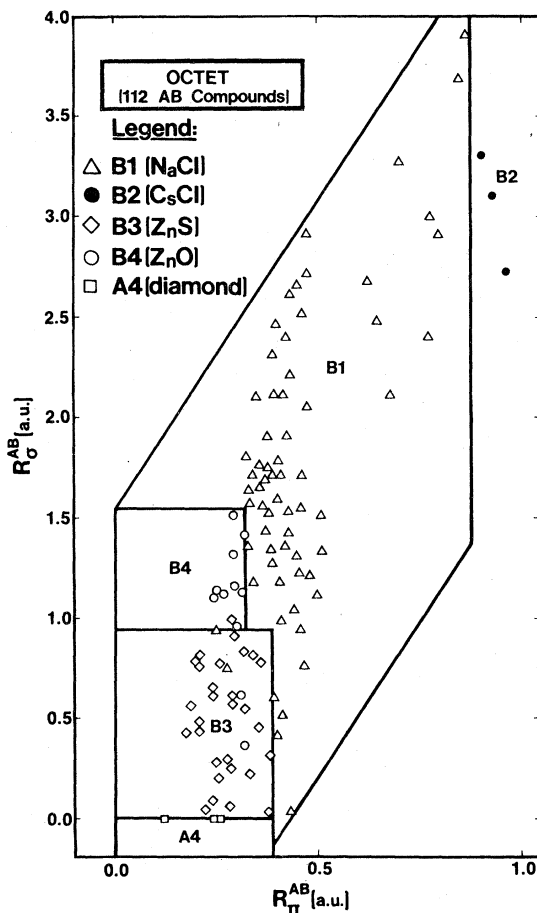


FIG. 19. Structural separation plot for the 112 binary octet compounds  $A^N B^{(8-N)}$ , obtained with the density-functional orbital radii, with

$$\begin{aligned} R_{\sigma}^{AB} &= |(\gamma_p^A + \gamma_s^A) - (\gamma_p^B + \gamma_s^B)|, \\ R_{\tau}^{AB} &= |\gamma_p^A - \gamma_s^A| + |\gamma_p^B - \gamma_s^B|. \end{aligned}$$

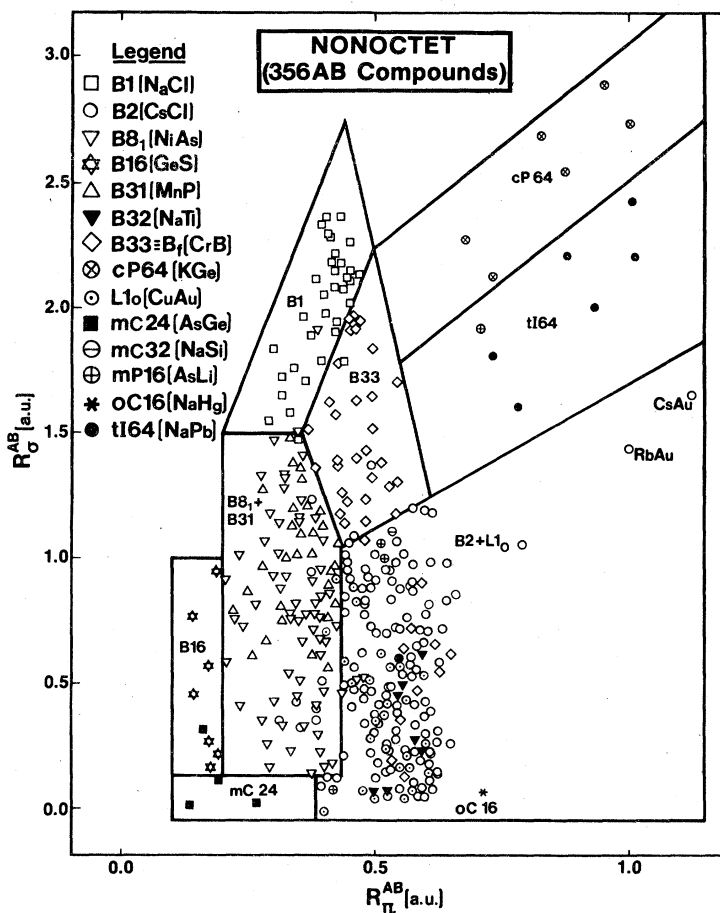


FIG. 20. Structural separation plot for the 356 binary nonoctet compounds, obtained with the density-functional orbital radii, with  $R_G^{AB} = |(\gamma_p^A + \gamma_s^A) - (\gamma_p^B + \gamma_s^B)|$ ,  $R_T^{AB} = |\gamma_p^A - \gamma_s^A| + |\gamma_p^B - \gamma_s^B|$ .

of assessing the true success of the method.

The remarkable result of these plots is that with the same linear combination of atomic-orbital radii, most of the structures to which the 468 compounds appearing in these plots belong can be separated. The relative locations of the structural domains seems chemically reasonable. Hence, the B27-B33 (coordination number CN=7) is intermediate between the B1 structure (CN=6) and the B2-L1<sub>0</sub> structures (CN=8). The mostly metallic nonoctet compounds appear separate from the non-metallic regime to the right (cP64, tI64, mC32, mP16, oC16), etc. Within single structural groups one similarly finds a chemically reasonable ordering of compounds, e.g., polymorphic compounds (such as SiC) appear near border lines, zinc-blende-rocksalt pairs that intertransform at low pressure appear along the B3-B1 separating line, etc. Note that even the wurtzite-zinc-blende structures, which only differ starting from the third-nearest neighbors, are well separated. How-

ever, there are a number of crystallographically closely related structures that overlap: I am unable to separate the nonoctet crystal type CsCl (B2) from the CuAu (L1<sub>0</sub> structure), the NiAs type (B8<sub>1</sub>) from the MnP type (B31), and the CrB type (B33) from the FeB type (B27), etc. For clarity of display, I show the extra 81 compounds separately in Fig. 21, however, using precisely the same separating lines as used for all other nonoctet compounds (Fig. 20).

It is not surprising that some of these structural pairs overlap. For instance, the B27 and B33 structures have a common structural unit consisting of a row of trigonal prisms of atom A stacked side by side and centered by a zigzag chain of B atoms.<sup>98(a)</sup> The structural similarity between CsCl (B2) and CuAu (L1<sub>0</sub>) has been discussed by Hume-Rothery and Raynor,<sup>9</sup> the relation between the NiAs (B8<sub>1</sub>), MnP (B31), and the FeSi (B20) structures by Schubert and Eslinger,<sup>99</sup> and that between the CsCl (B2), AuCd (B19), and CuTi (B11) by Pear-

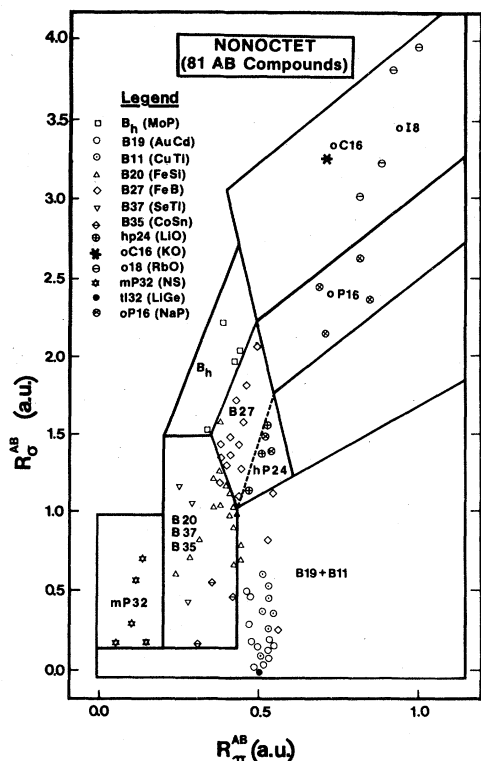


FIG. 21. Structural separation plot for the 81 binary nonoctet compounds, obtained with the density-functional orbital radii, with

$$R_{\sigma}^{AB} = |(\gamma_p^A + \gamma_s^A) - (\gamma_p^B + \gamma_s^B)|, \quad R_{\tau}^{AB} = |\gamma_p^A - \gamma_s^A| + |\gamma_p^B - \gamma_s^B|.$$

son.<sup>7</sup> In fact, examination of the thermochemical data (Refs. 12 and 13 and references therein) indicates that if a certain compound exists in two of these related structures at somewhat different temperatures, the difference in their standard heats of formation is often as small as 0.3 kcal/mole. (For example, AgCd in the B19 structure has  $\Delta H = 0.094 \pm 0.004$  eV, whereas the B2 structure has a heat formation of  $0.080 \pm 0.004$  eV.) Also, some of these presently unseparated structures indeed appear as mixtures when prepared from the melt (e.g., as noted by Hohnke and Parthé,<sup>98(a)</sup> both the B27 and the B33 structures are frequently found in the same arc-melted buttons of these compounds).

Since the publication of a preliminary report of this work,<sup>57</sup> which included 495 compounds, we have been made aware of the crystal structures of 54 more octet and suboctet compounds as well as 16 new superoctet compounds (i.e., a total of 565 compounds). We find that the lines separating the structural domains of the octet and suboctet compounds need not be changed relative to their previous assignment<sup>57</sup> to incorporate the 54 new com-

pounds. All the superoctet compounds (a total of 34) could be separated clearly as well (Fig. 22 and discussion below). This illustrates the predictive ability of the present approach.

If one is to consider the pairs of related crystal structures mentioned above as belonging to single generalized structural groups, the total number of misplaced compounds (5 octet and 32 nonoctet) forms only 7% of the total data base of binary compounds. The present theory is hence more than 90% successful.

### B. Discussion of "misplaced" compounds

The compounds that are misplaced in the present theory (i.e., their  $\{R_{\sigma}^{AB}, R_{\tau}^{AB}\}$  coordinates place them in a different structural domain than that reported in the literature surveyed) are listed in Table III together with their  $\{R_{\sigma}^{AB}, R_{\tau}^{AB}\}$  coordinates. In cases where a compound appears in overlapping domains or close to a border line, we indicate all the pertinent structures. Given their  $\{R_{\sigma}^{AB}, R_{\tau}^{AB}\}$  coordinates, the reader can conveniently identify them on structural plots.

The list of misplaced compounds shows a number of interesting features. At least two compounds, CuF (Table III, No. 1) and FeC (No. 16), reported to have the B3 (Ref. 90) and B1 (Ref. 92) structures, respectively, probably do not exist at all [for CuF see Ref. 100; for FeC, Ref. 101(a)]. Their misplacement in the present theory is hence a gratifying feature. Similarly, while OsSi (No. 11) is sometimes reported to have the B2 structure<sup>92</sup> and appears in our plots in the B20 domain (No. 11 in Table III), it is known to actually have the B20 structure and appears in B2 only with impurities.<sup>101(b)</sup> In addition, the compound PtB (No. 18 in Table III) which has been reported to have the NiAs (B8<sub>1</sub>) structure<sup>92</sup> and is placed in our plots in an entirely unrelated structural domain, has been found to have an anti-NiAs structure.<sup>101(b)</sup> NiY (No. 30) was reported in 1960 [Ref. 93(b), p. 678] to have the orthorhombic B27 structure, in conflict with the prediction of the present scheme, while in 1964 [Ref. 93(c), p. 561] it was concluded, that it is actually monoclinic with a  $P2_1/a$  space group. It seems that no clear identification for this structure is yet available. While HfPt (No. 21) is identified in most sources as having a B33 orthorhombic structure, a deformed B2 modification has also been reported [e.g., Ref. 93(c), p. 419]. Similarly, AuBe (No. 15) has been reported in 1947 to have the B20 structure [e.g., Ref. 93(b), p. 83] while in 1962 [e.g., Ref. 93(c), p. 64] it has been identified as tetragonal. AuLa (No. 29) has been reported to transform from its high-temper-

TABLE III. Compounds which are misplaced in the present theory (out of a total of 565).

Compound	Expected structure	Structural domain(s) in which it is found	$R_g^{AB}$ (a.u.)	$R_f^{AB}$ (a.u.)
Octet				
1. CuF	B3	B1	1.635	0.375
2. MgS	B1	B3	0.93	0.25
3. BeO	B4	B1-B3	0.615	0.305
4. MgTe	B4	B1-B3	0.36	0.32
5. MgSe	B1	B1-B3-B4	0.745	0.285
Nonoctet				
1. CoAl	B2	B8 <sub>1</sub> -B31-B20	0.345	0.315
2. FeAl	B2	B8 <sub>1</sub> -B31-B20	0.435	0.345
3. NiAl	B2	B8 <sub>1</sub> -B31-B20	0.505	0.395
4. CoGa	B2	B8 <sub>1</sub> -B31-B20	0.325	0.355
5. FeGa	B2	B8 <sub>1</sub> -B31-B20	0.415	0.385
6. NiGa	B2	B8 <sub>1</sub> -B31-B20	0.485	0.435
7. NiIn	B2	B8 <sub>1</sub> -B31-B20	0.13	0.43
8. MnIn	B2	B8 <sub>1</sub> -B31-B20	0.17	0.41
9. CoPt	L1 <sub>0</sub>	B8 <sub>1</sub> -B31-B20	0.68	0.40
10. TiAl	L1 <sub>0</sub>	B8 <sub>1</sub> -B31-B20	0.905	0.415
11. OsSi	B2	B8 <sub>1</sub> -B31-B20	1.23	0.37
12. CoBe	B2	B8 <sub>1</sub> -B31-B20	0.94	0.38
13. PdBe	B2	B33-B27	1.37	0.49
14. NaPb	tI64	B2-L1 <sub>0</sub> -B32	0.56	0.52
15. AuBe	B20	B1-B33-B27	1.58	0.44
16. FeC	B1	B1-B8 <sub>1</sub> -B31	1.47	0.35
17. TiB	B1	B1-B33-B27	1.785	0.445
18. PtB	B8 <sub>1</sub>	B1-B33-B27	1.905	0.385
19. IrPb	B8 <sub>1</sub>	B8 <sub>1</sub> -B31-B2	0.538	0.478
20. AgCa	B33	B1-L1 <sub>0</sub>	0.625	0.645
21. HfPt	B33	B2-L1 <sub>0</sub>	0.21	0.53
22. NiHf	B33	B2-L1 <sub>0</sub>	0.73	0.57
23. NiLa	B33	B2-L1 <sub>0</sub>	0.90	0.59
24. NiZr	B33	B2-L1 <sub>0</sub>	0.645	0.555
25. PtLa	B33	B2-L1 <sub>0</sub>	0.38	0.55
26. RhLa	B33	B2-L1 <sub>0</sub>	0.56	0.63
27. ZrPt	B33	B2-L1 <sub>0</sub>	0.125	0.515
28. PdLa	B33	B2-L1 <sub>0</sub>	0.63	0.62
29. AuLa	B27-B33	B2-L1 <sub>0</sub>	0.42	0.57
30. NiY	B27	B2-L1 <sub>0</sub>	0.76	0.56
31. PtY	B27	B2-L1 <sub>0</sub>	0.24	0.52
32. LaCu	B27	B2-L1 <sub>0</sub>	1.04	0.61

ature B33 form to a low-temperature B27 form (both orthorhombic) at about 660 °C, while in 1963 [Ref. 93(c), p. 73] it is indicated to have the cubic B2 form. It is hence clear that for some of the misplaced compounds, it is not yet obvious whether their misplacement is real. For the other compounds appearing in Table III, their misplacement in the present phase diagrams is real and brings up a number of interesting observations.

The octet compounds MgS and MgSe have a

NaCl (B1) structure but appear in our plot in the ZnS (B3) domain, near the B1 border. Experimentally (e.g., Ref. 102) it is found that the (normalized) free energy of the B3-B1 phase transition for these compounds is nearly zero.

A large number of the other misplaced compounds have unusual properties. Two such groups of compounds show *systematic* unusual properties: the six Al and Ga compounds with the magnetic 3d transition elements (CoAl, CoGa, FeAl, FeGa, NiAl, and NiGa) and the group of ten CrB and three FeB structures (AgCa, HfPt, NiHf, NiLa, NiZr, PtLa, RhLa, ZrPt, PdLa, and AuLa, and NiY, PtY, and LaCu, respectively).

The first group has the CsCl (B2) structure but appears in the present theory in the domain of the NiAs-MnP-FeSi structures. Their electric and magnetic properties have been studied intensively in the last few years (e.g., Refs. 103-110). It appears that these compounds are stabilized by the presence of defects, and they have a large, stable range of composition (45 at. %-55 at. %), with abrupt changes in many physical properties near stoichiometric composition. Susceptibility measurements as a function of magnetic field show ferromagnetic impurities and antistructure defects in such materials. More importantly, a slight nonstoichiometry often leads to the formation of local magnetic moments. These results indicate (e.g., Ref. 110) that such slightly off stoichiometric materials are in effect spin-glasses at low temperatures. Their magnetic behavior is intermediate between that of the independent magnetic-impurity problem (Kondo effect) and that characteristic of antiferromagnetic or ferromagnetic systems having long-range order due to strong magnetic interactions. It is interesting to note that this subgroup of compounds exhibiting stable intrinsic defects leading to magnetic moments, are displaced in the structural plots from the largely nonmagnetic B2 domain to the B8<sub>1</sub> region in which many of the *stoichiometric* alloys have permanent local moments. There are indications that this subgroup of compounds have certain structural anomalies: Many authors report that the B2 aluminides could not be obtained as a single phase, and in diffraction the B2 pattern could not be separated from other diffraction lines not belonging to this structure.<sup>97</sup> It was suggested (Schob and Parthé)<sup>97</sup> that many of these compounds are only *metastable* in the B2 structure. In a recent diffraction study<sup>108</sup> it was discovered that strong distortions occur around the Co sublattice sites in CoGa due to intrinsic vacancies. Similarly, a recent calculation<sup>104(b)</sup> of the ordering energy in FeGa using a Bragg-Williams model, yielded very small interaction parameters

of 0.049 and 0.03 eV (i.e.,  $\sim 2 - 1kT$ ) for first and second neighbors, respectively. It is intriguing that the present orbital-radii scheme has the ability of identifying such unusual phenomena in a few of the 122 tabulated *B2* nonoctet compounds.

Our scheme suggests that similar irregularities may occur in NiIn and TiAl and perhaps even in CoBe, but to a much smaller extent, since these compounds are only marginally misplaced in the present theory. Indeed, the absorption spectra of NiIn in the 0.7–5.5-eV range<sup>111</sup> indicate almost no change with composition in its Drude regime as well as above it, suggesting a constant number of electrons per cell due to the defect structure. This suggests that many of the unusual magnetic and structural properties found in the FeAl, FeGa, CoAl, CoGa, NiAl, NiGa group may also be found in NiIn.

The second large group of misplaced compounds (numbers 20–32 in Table III) form a distinct structural group. Schob and Parthé,<sup>97</sup> Rieger and Parthé,<sup>96</sup> and Hohnke and Parthé<sup>98(a)</sup> have indicated that all CrB (*B33*) and FeB (*B27*) compounds can be separated into two groups: group I, in which a transition-metal atom combines with an s-p element (B, Si, Ge, Al, Ga, Sn, or Pb), and group II, in which a transition element from the third or fourth group combines either with another transition element from group 8 or from the Cu group. It was found that the individual trigonal prisms in both the FeB and the CrB structures have different relative dimensions in groups I and II. In particular, group I of the CrB structure shows a "normal" *a/c* ratio greater than 1, but group II compounds show a compressed prism with *a/c* < 1. Only three compounds belonging to group I (HfAl, ZrAl, and YAl) have *a/c* < 1. We find that *all of the CrB and FeB compounds that belong to group II are misplaced by our theory into the bordering CsCl domain*, whereas the three group-I compounds that have *a/c* < 1 (much like group-II compounds) are correctly placed. Hence, the present approach is sufficiently sensitive to separate the true physical irregularity even when simple structural factors such as the *a/c* ratio lead to the wrong conclusion. From the results of the present approach, it would seem that group-II compounds of the FeB and CrB structures should properly be identified as a separate group. As a result, if the errors made by the present theory for the latter group of compounds, as well as the errors in the 1–8 (Table III) local-moment materials are regarded as *systematic irregularities*, the remaining true errors amount to only 2% of the total data base.

The placement of a number of *B33* and *B27* orthorhombic compounds in the CsCl (*B2*) region

of the present structural plots has an interesting implication on their electronic structure. The cubic *B2* structure of intermetallic compounds containing a magnetic element is stabilized by a partial ionic character and equiatomic composition. The experimental proof for that is given by the fact that the *B2*-type FeTi compounds has an almost vanishing atomic moment for Fe, indicating an ionic electron transfer which leads to a nearly zero spin polarization. Any deviation from stoichiometric composition leads to lattice distortions and defect structures attempting to accommodate the local magnetic interactions. Hence, the normally *B2* compounds FeAl, FeGa, NiAl, NiGa, CoAl, and CoGa may be distorted by off-stoichiometry and are indeed displaced in the structural plots. Similarly, some of the *B2*-displaced *B33* compounds (e.g., Table III No. 24, NiZr) do exist in a *B2*-type phase<sup>98(b)</sup> but may be distorted to a orthorhombic *B33* phase due to off-stoichiometry. Simultaneous measurements of the composition dependence of the Curie point and structural distortions may elucidate this point.

The remaining misplaced compounds may also have unusual properties; NaPb (No. 14) has an unusual structure with 64 atoms per cell resembling a molecular crystal with interacting Pb<sub>4</sub> tetrahedra<sup>112</sup> and IrPb (No. 19), according to Miedema's model,<sup>9</sup> has a positive heat of formation of about 1 kcal/mole. Similarly, AgCa (No. 20) has been recently discovered<sup>113</sup> to be one of the only known glass-forming materials that do not contain a transition or actinide element. It has also been noted<sup>43</sup> that the ratio of anion-anion to cation-anion distances in AgCa is almost an order of magnitude smaller than in all other non-transition-metal *B33* compounds, and that unlike the latter group of compounds it has catalytic properties in redox reactions.

CoPt (No. 9) has a tetragonal *L1<sub>0</sub>* structure but is displaced in the structural plots into the *B8<sub>1</sub>* domain, much like the FeAl, FeGa, CoAl, CoGa, NiAl, NiGa group. By quenching and annealing it below its order-disorder temperature in the presence of a magnetic field, it develops a uniaxial magnetic anisotropy leading eventually to a single-ordered system having its tetragonal axis in the direction of the applied magnetic field.<sup>114</sup> This material forms an excellent digital magneto-optic recording system.<sup>115</sup> Among its other structural peculiarities<sup>116</sup> it has been noted<sup>117</sup> that the *c/a* ratio calculated from the position of the main diffraction lines is considerably different from the *c/a* ratio evaluated from the superlattice lines, suggesting that this crystal actually consists of domains of different long-range order and

hence different tetragonalities.

It is interesting to note that the present scheme also predicts unusual *electronic properties* of compounds belonging to the same structural group. For instance, the  $B2$  compounds CsAu and RbAu that appear in Fig. 20 as isolated from the other 147  $B2 + L1_0$  suboctet compounds have semiconducting properties<sup>118</sup> while all other suboctet compounds belonging to these structures seem to be metals. A recent calculation of the electronic band structure of CsAu (Ref. 119) has indicated that if relativistic corrections are neglected, CsAu appears to be a metal, which disagrees with experiment, whereas the inclusion of relativistic effects lowers the Au  $s$  valence band to form a semiconductor. It is remarkable indeed that such complicated electronic-structure factors are required in quantum-mechanical band-structure calculations to reveal the unusual semiconducting behavior suggested here simply by the atomic-orbital radii.

If the predictive power of the present orbital-radii scheme in relation to unusual *electronic properties* is not accidental, it would be interesting to speculate on its consequences. One would guess, for instance, that all suboctet *non-transition-element* compounds having  $R_{\pi}^{AB}$  larger than roughly 0.7 a.u. are nonmetals. This includes not only the known nonmetallic compounds belonging to the LiAs group (KSb, NaGe, NaSb, but not LiAs) and the KGe group (CsGe, CsSi, KGe, RbGe, and RbSi whereas KSi is a borderline case), but also the  $tI64$  (NaPb) group (CsPb, CsSn, KPb, KSn, RbPb, and RbSn, but not NaPb), the  $B2$  compounds LiAu and LiHg, the  $L1_0$  compound NaBi, the  $oC16$  compound NaHg, and the  $mC32$  compound NaSi. In the sequence of alkali-gold compounds LiAu, NaAu, KAu, RbAu, and CsAu, one would similarly predict that the transition between metallic and insulating behavior occurs between NaAu and KAu.

Another demonstration of the usefulness of the present approach in systematizing properties within a given structural group is the application to the  $c/a$  axial ratio of the NiAs compounds. The measured axial ratios of the  $B8_1$  compounds of Ti, V, Cr, Mn, Fe, Co, and Ni with S, Se, Te, As, Sb, and Bi show very large variations around the "ideal" value of  $c/a = 1.633$  (ranging from 1.95 for TiS to 1.25 for FeSb). Defining the deviation from this value as  $\Delta = c/a - 1.633$ , one immediately recognizes that the known semiconductors in this group have mostly  $\Delta > 0$ , whereas the metallic NiAs compounds usually have  $\Delta < 0$ . One then finds, using the ionicity coordinate  $R_{\sigma}^{AB}$ , that compounds with  $R_{\sigma}^{AB} \leq 0.9$  a.u. have  $\Delta < 0$  as the size mismatch of the effective cores  $|(r_p^A + r_s^B)|$

$|(r_p^B + r_s^B)|$  is too large to accommodate an ionic structure. NiS (with  $\Delta = 0.073$  and  $R_{\sigma}^{AB} = 1.08$ ) is the only exception to this rule. A similar correlation of  $\Delta$  with  $R_{\sigma}^{AB}$  exists for the wurzite  $B4$  compounds,<sup>43, 58</sup> although the range of  $\Delta$  is an order of magnitude smaller than it is in the  $B8_1$  compounds.

### C. Superoctet compounds and additional structural plots

The relative orientation of the structural domains in Figs. 19–21 suggest that no *single* coordinate will suffice to produce a complete topological separation between all structures. Since, however, the area of the  $R_{\sigma}^{AB}$  vs  $R_{\tau}^{AB}$  plane seems to be more or less bound (e.g.,  $\approx 3$  a.u.<sup>2</sup> in Fig. 20), when extra compounds are added (i.e., compare the 495 compounds included in Ref. 57 with the 559 compounds in Figs. 19–21), it is likely that the two-dimensionality of this finite  $R_{\sigma}^{AB}$ - $R_{\tau}^{AB}$  space will eventually preclude the delineation of further structures. One may hence expect that for some critical number of structures and compounds, a third coordinate may be needed. Such a generalized multidimensional resolution of structural groups may also resolve some of the remaining discrepancies in the present theory. Our present approach, however, is aimed at demonstrating the extent of structure delineation possible with the minimum number of two coordinates using the simplest possible separating lines.

One simple example for an additional coordinate is the classical<sup>4</sup> valence-electron concentration (VEC), measuring for the binary  $AB$  system the total number of valence electrons  $Z_v^A + Z_v^B$  [cf., Eq. (10)] in the compound. In the semiclassical approaches to structure it is known that whereas the VEC value alone does not separate different crystal structures, compounds with the same valence-electron number often belong to the same broad structural groups.<sup>4</sup> One can use this additional coordinate together with our orbital radii to obtain a better structural resolution of the marginally resolved structures, and at the same time provide a clear structural delineation of all *superoctet* (i.e.,  $Z_v^A + Z_v^B > 8$ ) compounds. As with the suboctet compounds, no previous approach has succeeded in systematizing these complex crystal structures.

We find that while the definition of the structural coordinates  $R_{\tau}^{AB}$  and  $R_{\sigma}^{AB}$  [Eq. (21)] used for the octet (Fig. 19) and mostly suboctet (Figs. 20 and 21) compounds yields an overall separation also of the superoctet compounds, a more sensitive delineation is obtained with the slightly modified coordinates  $R_1 = |r_p^B - r_p^A|$  and  $R_2 = (R_{\tau}^{AB})^{-1}$  suggested by Littlewood.<sup>120</sup> Here,  $R_1$  is a measure



GaSe, GeTe, SnTe, InSe), and the orthorhombically distorted B1 compound TlF. It is seen that the seven different structures of the VEC=9 compounds, as well as the six different VEC=10 structures, are very clearly resolved, the only exception out of these 34 compounds being the B37 compound TlS which is marginally displaced into the neighboring  $hP8-hR2$  domain [Fig. 22(a)].

It is important to emphasize that the ability to separate structures shown by the present orbital radii (Figs. 19–21) is far from being trivial or accidental. This is demonstrated in Figs. 23–25, where structural plots are presented for some of the nonoctet compounds using different coordinates. We use Miedema's<sup>9</sup> coordinates,  $R_2 = |\phi_A^* - \phi_B^*|$  and  $R_1 = |n_A^{*1/3} - n_B^{*1/3}|$  in Fig. 23, where  $\phi_A^*$  and  $n_A^{*1/3}$  are the effective elemental work function and cell-boundary density to the power of  $\frac{1}{3}$ . Those coordinates were extremely successful in predicting the signs (and often the magnitudes) of the heats of formation of more than 500 compounds.<sup>9</sup> In Fig. 24, we present a Mooser-Pearson<sup>4</sup> plot, where  $R_2$  is the elemental electronegativity difference, and  $R_1$  is the average principal quantum number. In Fig. 25, we give a plot

using Shaw's parameters,<sup>72</sup> where  $R_2$  is the elemental electronegativity difference and  $R_1 = \frac{1}{2}(Z_A + Z_B)/[\frac{1}{2}(n_A + n_B)]^3$ , where  $Z_A$  and  $n_A$  are the atomic number and the principal quantum number of the outer valence orbital, respectively.

In a Miedema plot (Fig. 23), one notices a rough separation of the B1 and B8<sub>1</sub> structures (CsAu and RbAu appear, as in our case, at high  $\Delta\Phi^*$ ,  $\Delta n^{*1/3}$ ), whereas most other structures are nearly indistinguishable. This illustrates the great difficulty in carrying the success of a theory that predicts *global binding energies*  $\Delta E_0$  into the prediction of *structural energies*  $\Delta E_s$  (cf. Sec. I).

The Mooser-Pearson plot for these compounds (Fig. 24) appears visually as if only 104 compounds (i.e., isolated points) are plotted. In fact, it includes 360 compounds belonging to 14 different structures. This strong overlap of different structures on the same ( $R_1$ ,  $R_2$ ) coordinate reflects the insensitivity of the scale to separating such structures. A somewhat better separation is evident using Shaw's parameter (Fig. 25), but the overlap of different structures is still extremely large.

It is likely that one could construct first-prin-

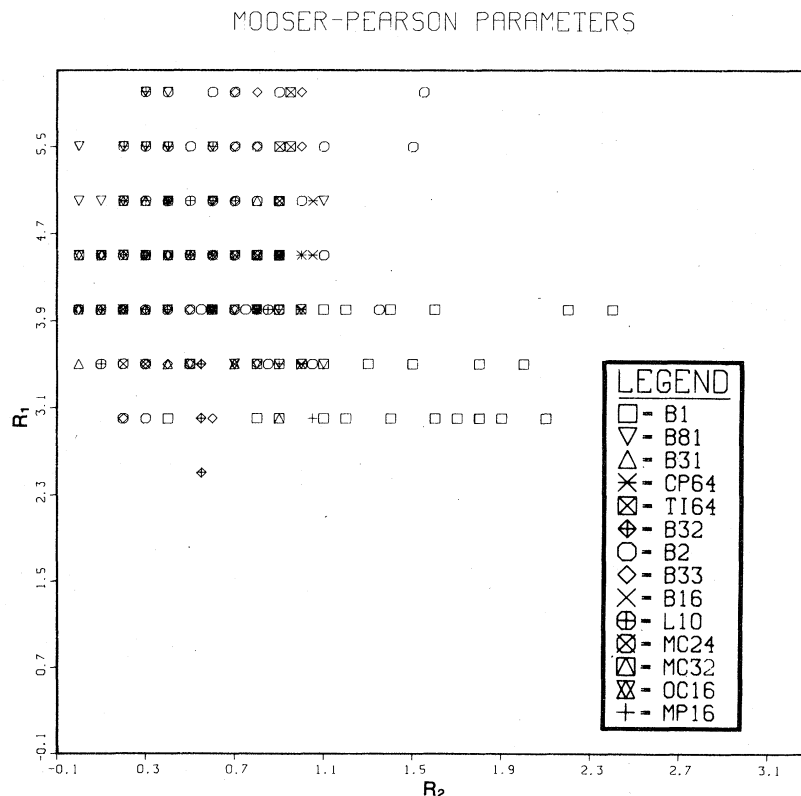


FIG. 24. Mooser-Pearson (Ref. 4) plot for 360 nonoctet compounds.  $R_2 = |X_A - X_B|$ ;  $R_1 = \frac{1}{2}(n_A + n_B)$ , where  $X_A$  and  $n_A$  are the elemental electronegativity and principal quantum number of the outer orbital, respectively.

## Shaw Parameters

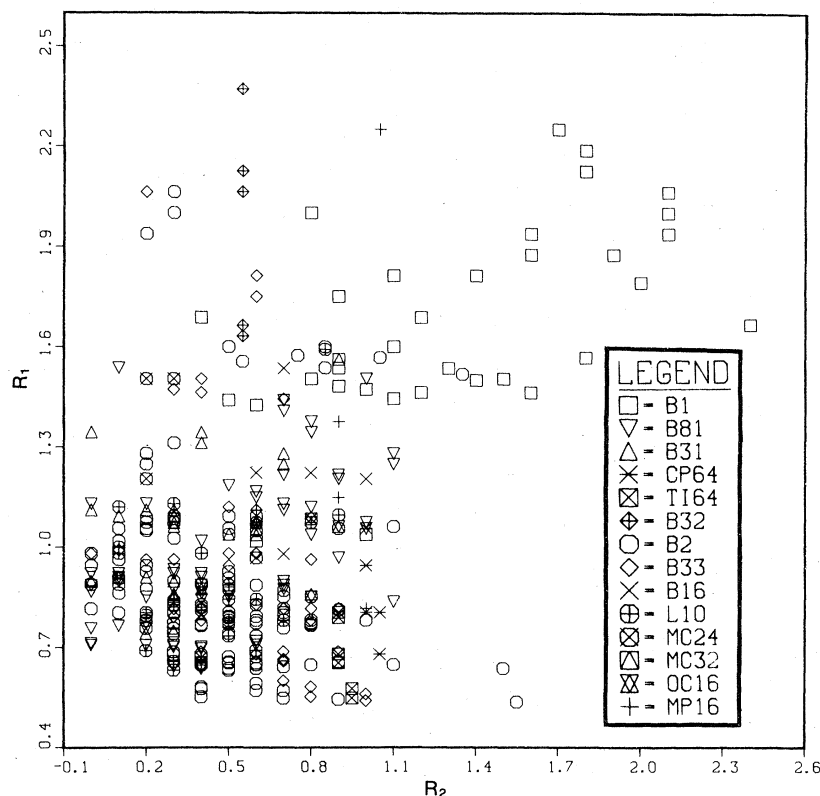


FIG. 25. Structural separation plot for the nonoctet compounds using Shaw's (Ref. 72) coordinates  $R_2 = |X_A - X_B|$ ,  $R_1 = \frac{1}{2}(Z_A + Z_B) / [\frac{1}{2}(n_A + n_B)]^3$ , where  $X_A$ ,  $Z_A$ , and  $n_A$  are the elemental electronegativity, atomic number, and principal quantum number of the outer orbital, respectively.

ciples atomic pseudopotential using somewhat different procedures than have been used here (Sec. III A) for defining the pseudo-wave-functions. While this would result in a different set of orbital radii, they will most likely scale with the present set of radii. Consequently, one may expect that the systematization of the crystal structures, based on such radii, will be essentially unchanged.

#### D. Discussion

As indicated in the Introduction, the success of the  $s$  and  $p$  orbital-radii scheme in correctly predicting most of the structural regularities of  $AB$  compounds suggests that the *structural part*  $\Delta E_s$  of the cohesive energy may be dominated by  $s$ - $p$  electrons, even in transition-metal systems. The effect of the  $d$  electrons then enters indirectly via the screening term in Eq. (16). This points to the possibility that while the localized  $d$  electrons determine central-cell effects and hence also the regularities in the structure-insensitive part  $\Delta E_0$

of the total cohesive energy  $\Delta E = \Delta E_0 + \Delta E_s$  (with  $\Delta E_0 \gg \Delta E_s$ ), the longer-range  $s$ - $p$  wave functions are responsible for the stabilization of a certain complex space-group arrangement over another.<sup>57</sup> This may seem as a somewhat surprising result, in view of the fact that the resonant tight-binding models<sup>22-24</sup> have explained the periodic trends in  $\Delta E_0$  of both elemental and alloyed transition-metal systems by considering changes in the rectangular distribution of the one-electron  $d$  energy levels alone. The two views need not, however, be contradictory. This point is discussed below.

The analysis of molecular and crystal binding in variational quantum-mechanical theories in terms of the predominance of a certain subset of wave functions with a well defined (majority) angular symmetry (e.g.,  $s$ ,  $p$ , and  $d$ ), is inherently qualitative. In fact, while the systematic errors introduced by such approximations are often small enough on the scale of  $\Delta E_0$  (so that trends in global cohesive energies  $\Delta E$  may be reproduced), they are frequently of the order of  $\Delta E_s$  itself, or even larger. For example, the analysis

of the computed formation energy  $\Delta H$  of NiAl in terms of the differences  $\Delta_2$  in the one-electron  $d$  orbital ( $l=2$ ) energies of the compound and the elemental solids, shows that  $\Delta_2$  differs by 30% from  $\Delta H$ . Such theories will be appropriate for predicting trends in structural energies only in the rare event where the structural energy  $\Delta E_s$  is much larger than about 30% of the global binding energy.

Whereas the *variational* total energy of a polyatomic system is not even decomposable into atomic site and angular momentum compounds, under suitable approximations the *virial* total energy (i.e., the negative of one-half the kinetic energy) is amenable to such a partitioning. However, in cases where such a decomposition has been attempted,<sup>121</sup> one has obtained the somewhat counter intuitive result that changes in the (outer) core orbitals in forming the solid from atoms are mainly responsible for the cohesion.

Such results have encouraged the utilization of the difference in the sum of one-electron energies  $\Delta_i = \sum_i \epsilon_{ii}^{AB} - \sum_i \epsilon_{ii}^A - \sum_i \epsilon_{ii}^B$  between the compound  $AB$  and its constituents  $A$  and  $B$ , as a measure of the cohesive or formation energy of  $AB$ .<sup>22-24</sup> This permits the decomposition of binding energies into angular components, from which one may hope to assess the dominance of a certain term. While it was long known that  $\sum_i \Delta_i$  rarely shows a minimum as a function of structural coordinates unless  $\epsilon_i$  are empirically parametrized (as in the extended Hückel method (e.g., Ref. 122 and references therein), Rudenberg<sup>123</sup> has discovered the remarkable result that *at equilibrium*, the total Hartree-Fock energy of a molecule equals approximately the sum of one-electron energies:  $E_{\text{HF}} \cong k_1 \sum_i \epsilon_i$ , where  $k_1$  is an empirical factor. This energy relation is based on an earlier discovery by Politzer<sup>124</sup> showing that  $E_{\text{HF}} \cong k_2 (V_{\text{en}} + 2V_{\text{nn}})$ , where  $V_{\text{en}}$  and  $V_{\text{nn}}$  are, respectively, the electron-nuclear and nuclear-nuclear potential energies and  $k_2 \cong \frac{3}{7}$ . These new energy relations have been recently investigated in great detail in the chemical literature.<sup>122-129</sup> The picture that emerges from these studies is that: (i) The errors made in approximating the total energy by sums of all of the occupied one-electron energies is very large on the scale of binding energies  $\Delta E$ , let alone molecular conformational (i.e., structural) energies  $\Delta E_s$ . Even the trends (i.e., differential errors) in going from one system to the other are often obscured by such approximations, unless the constants  $k_1$  and  $k_2$  are fine-tuned to take different values for atoms in different chemical environments. (ii) Whereas the Politzer-Rudenberg relations are valid only at the equilibrium geometry, additional corrections for non-

equilibrium terms still fail to make these energy relationships useful for finding approximate geometries of molecules. Despite such gross inaccuracies, it would seem that further analysis along these lines (e.g., Ref. 126) may be used to isolate in the future the major orbital contributions to binding energies.

The realization that simple differences in the sums of all occupied one-electron energy levels do not form an adequate measure to the chemical trends apparent in the total energy leads to two possible extensions. In the first approach<sup>130</sup> one represents the total energy as a sum of all occupied orbital energies plus an empirical classical strain-energy term which is adjusted to produce a minimum of the total energy at the observed structural parameters. While this strain-energy term is small, it is crucial for physically meaningful predictions for the structure dependence of the total energy. Its inclusion, however, no longer permits the decomposition of the total energy into angular momentum components.

The second approach assumes that the total heat of formation scales with the difference  $\Delta_i$  between the one-electron energy levels of the compound and its constituent elemental solids, but only a single  $l$  component (e.g.,  $d$ ) is isolated as relevant for this scaling relation.<sup>22-24</sup> The latter part of this statement is crucial: if one attempts, for instance, to approximate the trends in the heat of formation of compounds made of a transition and a simple element by  $\Delta_0 + \Delta_1 + \Delta_2$  rather than by  $\Delta_2$  alone, no meaningful correlation is found.<sup>131</sup> Williams *et al.*<sup>132</sup> have suggested an explanation for this scaling relation in terms of a near cancellation between the attractive Madelung interatomic potential and the repulsive intra-atomic Coulomb potential. If such a cancellation were to be exact, trends in  $\Delta_2$  alone would parallel those obtained from variational total-energy calculations. The basis of this approach is that whereas the Madelung term  $V_M^\alpha$  lowers (raises) the energy of states which occur predominantly on the negatively (positively) charged sublattice in an  $A^+B^-$  compound, charge transfer to the negatively charged species raises its intra-atomic Coulomb energy with respect to that of the positively charged species. Similar ideas were previously tested for simple binary compounds<sup>133</sup> by calculating the sums  $[\epsilon_A^+(Q) + V_M^+(Q)]$  and  $[\epsilon_B^-(Q) + V_M^-(Q)]$ , where  $\epsilon_A^+$  and  $\epsilon_B^-$  are orbital energies of species with formal charge  $Q$  and  $V_M^+$ ,  $V_M^-$  are the Madelung potentials at the respective atomic site. By varying  $Q$ , it was observed that indeed a large cancellation occurs between  $\epsilon_\alpha^+$  and  $V_M^+$ , but that the residue of this cancellation is as large as 10-20% of  $\epsilon_\alpha$  or  $V_M$ , and hence significant on the

scale of structural energy  $\Delta E_s$ . A similar result was recently reported<sup>131</sup> for NiAl.

One would therefore conclude that from the schemes proposed so far for decomposing binding energies into angular momentum contributions, it is impossible to deduce the dominance of any particular interaction (i.e.,  $d$  or  $s-p$ ) in determining structural regularities.

The lack of contradiction between Friedel's resonant tight-binding model and the significant structural role assigned to the  $s-p$  coordinates in the present model becomes obvious in considering the contributions entering the former theory: it may be that in binary  $AB$  compounds with large differences in the constituent  $d$ -band energies,  $E_d(A) \neq E_d(B)$ , the  $s-p$  contribution to the structural energy  $\Delta E_s$  is indeed dominant. If  $\Delta E_s$  is derived primarily from Brillouin-zone-induced changes in the gaps  $E_{BZ}$  and these gaps can be divided into two groups  $E_{BZ}^d$  and  $E_{BZ}^{s,p}$  (nonexistent in rectangular  $d$  density of states models),<sup>17-21</sup> then the dominant structural role of  $s-p$  electrons becomes evident if covalent hybridization leads to  $E_{BZ}^d \ll E_{BZ}^{s,p} < E_d(A) - E_d(B)$ .  $E_{BZ}^{s,p}$  is then expected to scale with  $R_{\tau}^{AB}$  much like the heteropolar gaps.

The relationship between the structural stability of a polyatomic system and the degree of repulsiveness of the effective atomic cores of the constituent atoms has been discussed in 1948 by Pitzer<sup>134</sup> in a remarkable paper preceding all pseudopotential theories. While one might have thought then naively that the electron-core attraction term  $-Z_v/r$  would lead to a strong penetration by valence electrons of the core regions of neighboring atoms, Pitzer has realized that the core electrons set up a repulsive potential with a characteristic radius inside which such a penetration is discouraged. Hence, the triple-bond energy of  $N \equiv N$  is much higher than that of  $P \equiv P$  (and the bond length in  $N \equiv N$  is significantly shorter than in  $P \equiv P$ ) because the repulsive core size of nitrogen is so much smaller than that of phosphorus. Similarly, the occurrence of multiple chemical bonds with first-row elements as compared with the rare occurrence of such bonds (with a small bond energy) with heavier atoms has been naturally explained in terms of the large repulsive core size of the latter elements. In addition, Pitzer noted that whereas Pauling<sup>5</sup> has suggested that single bond energies (e.g.,  $N-N$ ) should be roughly  $\frac{3}{4}$  of the tetrahedral bond energy (e.g.,  $C-C$ ), in fact the ratio of the two is closer to  $\frac{1}{2}$ . This discrepancy was simply explained<sup>134</sup> by the fact that the change from the bond angle of  $90^\circ$  characteristic of  $p$ -type single bonds, to a tetrahedral angle of  $109.5^\circ$  minimized in the latter case

the overlap with the repulsive core.

In the present orbital-radii approach, these ideas are realized in a simple manner. To first order, the change in energy per atom introduced by incorporating an atom in a polyatomic system is proportional to:

$$\delta E \sim \sum_l k_l \int \Delta \rho_l(r) [U_l(r) + \Delta(r)] dr, \quad (22)$$

where  $\Delta \rho_l(r)$  is the  $l$ th component of the charge redistribution,  $U_l(r)$  is the Pauli repulsive potential [Eq. (11)],  $\Delta(r)$  is the  $l$ -independent part of the atomic pseudopotential [Eq. (10)], and  $k_l$  are constants. The first  $\Delta \rho_l(r)U_l(r)$  term in Eq. (22) leads to a repulsive and angular-momentum-dependent contribution (for electron-attracting species) while the second term is isotropically attractive (for similar atoms). Neglecting for this simple argument the nonlinear dependence of the charge-density redistribution  $\Delta \rho_l(r)$  on  $U_l(r)$ , one notes that Pitzer's ideas on the destabilizing role of large-core atoms, as well as the relative stability of structures that minimize such repulsions through conformational changes in bond angles, are directly manifested in Eq. (22). One could further note that charge-redistribution effects occurring predominantly outside the pseudopotential core [where  $U_l(r) \approx 0$ ] do not contribute to such strongly directional repulsive terms. It would seem reasonable that the dominance of the centrifugal barrier at small distances from the origin will cause the charge-redistribution effects in the high angular momentum components of the density to be confined to regions outside  $U_l$  (i.e.,  $r \gtrsim r_l$ ). This simple picture clearly indicates the important structural role played by the  $r_s$  and  $r_p$  coordinates, as compared to higher angular momentum orbital coordinates.

## VI. SUMMARY

It has been demonstrated that the pseudopotential theory in its present nonempirical density-functional form is capable of providing transferable atomic pseudopotentials  $v_{ps}^{(l)}(r)$  that can be used both for performing reliable quantum-mechanical electronic-structure calculations<sup>58,77-83</sup> and for defining semiclassical-like elementary length and energy scales  $\{r_{ij}\}$ . The resulting radii correlate with a large number of classical constructs that have been traditionally used to systematize structural and chemical properties of many systems. At the same time, the orbital radii derived here are capable of predicting the stable crystal structure of the 112 octet compounds (Fig. 19), 419 suboctet compounds (Figs. 20 and 21), and 34 superoctet compounds (in Fig.

22) with a remarkable success, exceeding 95%. The compounds for which the present theory does not predict the correct crystal structure are analyzed and found to be largely characterized as defect structures with many unusual electronic, magnetic, and structural properties.

#### ACKNOWLEDGMENTS

I would like to thank A. N. Bloch, M. L. Cohen, and J. C. Phillips for inspiring and useful discussions. Special thanks are due to E. Parthé and F. Hulliger for reviewing the present compilation of crystal structures. I am grateful to L. Pauling for bringing Ref. 134 to my attention and discussing related work.

#### APPENDIX

This appendix presents an alphabetic list of the stable structures of the binary  $AB$  compounds whose atoms belong to the first five rows of the Periodic Table. The headings include the *strukturberichte* symbol (or Pearson's symbol, if the former is unavailable), the space-group notation, and the crystal type, respectively. A single asterisk indicates that there exists an uncertainty in assigning the structure due to off-stoichiometry, superstructures, possible metastability, existence of a defect structure or a distorted structure. Two asterisks indicate that there exists another competing phase adjacent to it in the phase diagram. Structures not plotted in Figs. 19–22 are denoted by square brackets. For nontransition-element systems we indicate if the compounds are superoctet ( $A^N B^{10-N}$ ). We do not include in our list the hydrides (there is no hydrogen pseudopotential), some oxides and sulphides which do not occur in their stable form as monomeric binary compounds ( $\text{SiO}$ ,  $\text{SiS}$ , etc.), or binary systems which form continuous solutions or yet unknown structures.

The assignment of a compound as "octet" or "nonoctet" is sometimes arbitrary. Hence, the rocksalt-type  $MX$  compounds with  $M = \text{La}$ ,  $\text{Sc}$ , or  $\text{Y}$  ( $d^1 S^2$ ) and  $X = \text{O}$ ,  $\text{S}$ ,  $\text{Se}$ ,  $\text{Te}$  ( $S^2 P^4$ ) are sometimes assigned in the literature as nine-electron nonoctet systems, while frequently the  $d^1$  electrons of the group-III $B$  element are considered as "chemically inactive," leading to the assignment of these compounds as "octet" or "pseudo-octet." We have listed these compounds under octet, although this classification does not alter the quality of separation in the structural plots. The same considerations apply to compounds such as  $\text{MnS}$ ,  $\text{MnSe}$ , and  $\text{MnTe}$  which can be considered as pseudo-octet if the five  $d$  electrons of  $\text{Mn}$  are taken as "inactive."

For some compounds it is difficult to establish from the existing literature which structure out of

two competing structures is the most stable, e.g.,  $\text{AsCo}$  in the  $B8_1$  or  $B31$  structures or  $\text{RhSi}$  in the  $B20$  and  $B31$  structures. In all cases where such a "metastability" exists, we find that either the two structural groups are unseparable in the present theory (e.g.,  $B8_1$  and  $B31$ ) or that the compound occurs in our structural plots in the border of the two competing structures (see text).

#### Octet compounds

##### $B1, Fm\bar{3}m, \text{NaCl type}$

$\text{AgBr}$ ,  $\text{AgCl}$ ,  $\text{AgF}$ ,  $\text{BaO}$ ,  $\text{BaPo}$ ,  $\text{BaS}$ ,  $\text{BaSe}$ ,  $\text{BaTe}$ ,  $\text{CaO}$ ,  $\text{CaPo}$ ,  $\text{CaS}$ ,  $\text{CaSe}$ ,  $\text{CaTe}$ ,  $\text{CdO}$ ,  $\text{CsF}$ ,  $\text{HgPo}$ ,  $\text{KBr}$ ,  $\text{KCl}$ ,  $\text{KF}$ ,  $\text{KI}$ ,  $\text{LaAs}$ ,  $\text{LaBi}$ ,  $\text{LaN}$ ,  $\text{LaO}$ ,  $\text{LaP}$ ,  $\text{LaS}$ ,  $\text{LaSb}$ ,  $\text{LaSe}$ ,  $\text{LaTe}$ ,  $\text{LiBr}$ ,  $\text{LiCl}$ ,  $\text{LiF}$ ,  $\text{LiI}$ ,  $\text{MgO}$ ,  $\text{MgS}^{**}$ ,  $\text{MgSe}^{**}$ ,  $\text{NaBr}$ ,  $\text{NaCl}$ ,  $\text{NaF}$ ,  $\text{NaI}$ ,  $\text{RbBr}$ ,  $\text{RbCl}$ ,  $\text{RbF}$ ,  $\text{RbI}$ ,  $\text{ScAs}$ ,  $\text{ScBi}$ ,  $\text{ScN}$ ,  $\text{ScP}$ ,  $\text{ScS}$ ,  $\text{ScSb}$ ,  $\text{ScSe}$ ,  $\text{SrO}$ ,  $\text{SrPo}$ ,  $\text{SrS}$ ,  $\text{SrSe}$ ,  $\text{SrTe}$ ,  $\text{YAs}$ ,  $\text{YBi}$ ,  $\text{YO}$ ,  $\text{YN}$ ,  $\text{YP}$ ,  $\text{YS}$ ,  $\text{YSb}$ ,  $\text{YSe}$ ,  $\text{YTe}$ .

##### $B2, Pm\bar{3}m, \text{CsCl type}$

$\text{CsBr}$ ,  $\text{CsCl}$ ,  $\text{CsI}$ .

##### $B3, F\bar{4}3m, \text{ZnS type}$

$\text{AgI}$ ,  $\text{AlAs}$ ,  $\text{AlP}$ ,  $\text{AlSb}$ ,  $\text{BAs}$ ,  $\text{BN}^{**}$ ,  $\text{BP}$ ,  $\text{BePo}$ ,  $\text{BeS}$ ,  $\text{BeSe}$ ,  $\text{BeTe}$ ,  $\text{CSi}^{**}$ ,  $\text{CdPo}$ ,  $\text{CdTe}^{**}$ ,  $\text{CuBr}$ ,  $\text{CuCl}$ ,  $\text{CuI}^{**}$ ,  $\text{GaAs}$ ,  $\text{GaP}$ ,  $\text{GaSb}$ ,  $\text{HgTe}^{**}$  (also  $B9$ ),  $\text{InAs}$ ,  $\text{InP}$ ,  $\text{InSb}^{**}$ ,  $\text{MnSe}^{**}$ ,  $\text{ZnPo}$ ,  $\text{ZnS}^{**}$ ,  $\text{ZnSe}^{**}$ ,  $\text{ZnTe}^{**}$ .

##### $B4, P6_3mc, \text{ZnO type}$

$\text{AlN}$ ,  $\text{BeO}$ ,  $\text{CdSe}^{**}$ ,  $\text{CdS}^{**}$ ,  $\text{GaN}$ ,  $\text{HgSe}^{**}$  (also  $B9$ ),  $\text{HgS}^{**}$  (also  $B9$ ),  $\text{InN}$ ,  $\text{MgTe}$ ,  $\text{MnS}$ ,  $\text{ZnO}^{**}$ .

##### $A4, Fd\bar{3}m, \text{diamond type}$

$\text{C}$ ,  $\text{Ge}$ ,  $\text{Si}$ ,  $\text{Sn}$ .

#### Nonoctet compounds

##### $B1, Fm\bar{3}m, \text{NaCl type, suboctet}$

$\text{CoO}^{**}$ ,  $\text{CrN}$ ,  $\text{CrO}$ ,  $\text{FeC}^{**}$ ,  $\text{FeO}^{**}$ ,  $\text{HfB}$ ,  $\text{HfC}$ ,  $\text{HfN}$ ,  $\text{MnO}^{**}$ ,  $\text{MoC}^{**}$ ,  $\text{NbC}$ ,  $\text{NbN}^{**}$ ,  $\text{NbO}^*$ ,  $\text{NiO}^{**}$ ,  $\text{ScC}$ ,  $\text{TaC}^*$ ,  $\text{TaO}$ ,  $\text{TcN}^*$ ,  $\text{TiB}$ ,  $\text{TiC}^*$ ,  $\text{TiN}^*$ ,  $\text{TiO}^*$ ,  $\text{VC}$ ,  $\text{VN}^*$ ,  $\text{VO}^*$ ,  $\text{WC}^{**}$ ,  $\text{WN}^*$ ,  $\text{ZrB}$ ,  $\text{ZrC}$ ,  $\text{ZrN}$ ,  $\text{ZrO}$ ,  $\text{ZrP}^{**}$ ,  $\text{ZrS}^{**}$ .

##### $B1, Fm\bar{3}m, \text{NaCl type, superoctet:}$

$\text{BiSe}$ ,  $\text{BiTe}$ ,  $\text{PbPo}$ ,  $\text{PbS}$ ,  $\text{PbSe}$ ,  $\text{PbTe}$ ,  $\text{SnAs}$  (also  $\text{TiF}^{**}$ , an orthorhombically distorted  $B1$  structure).

##### $B2, Pm\bar{3}m, \text{CsCl type, suboctet}$

$\text{AgCd}$ ,  $\text{AgLa}$ ,  $\text{AgMg}$ ,  $\text{AgSc}$ ,  $\text{AgY}^*$ ,  $\text{AgZn}$ ,  $\text{AlSc}$ ,  $\text{AuMg}$ ,  $\text{AuSc}$ ,  $\text{AuY}$ ,  $\text{AuZn}^{**}$ ,  $\text{BaHg}$ ,  $\text{CaCd}$ ,  $\text{CaHg}$ ,  $\text{CaIn}$ ,  $\text{CaTl}$ ,  $\text{CdBa}$ ,  $\text{CdLa}$ ,  $\text{CdSc}$ ,  $\text{CdY}$ ,  $\text{CoAl}$ ,  $\text{CoBe}$ ,  $\text{CoCa}$ ,  $\text{CoGa}$ ,  $\text{CoHf}$ ,  $\text{CoSc}$ ,  $\text{CoZr}$ ,  $\text{CrPt}$ ,  $\text{CsAu}$ ,  $\text{CuBe}$ ,  $\text{CuSc}$ ,  $\text{CuY}$ ,  $\text{CuZn}^*$ ,  $\text{FeAl}$ ,  $\text{FeCa}$ ,  $\text{FeCo}$ ,  $\text{FeGa}$ ,  $\text{FeRh}^*$ ,  $\text{HfOs}^*$ ,  $\text{HgLa}$ ,  $\text{HgSc}$ ,  $\text{HgY}$ ,

InLa, IrAl, IrGa, IrSc, LaTl, LiAg\*\*, LiAu\*, LiHg, LiPb\*, LiTl, MgHg, MgLa, MgSc, MgSr\*, MgTl, MgY\*, MnAu\*, MnHg, MnIn, MnIr\* MnPd, MnPt\*\*, MnRh\*, MnZn\*, NiAl, NiBe, NiGa, NiIn\*\*, NiSc, NiZn\*\*, OsAl, OsSi\*\*, PdAl\*, PdBe, PdCu, PdIn, PdLi, PdSc, PtSc, RbAu, ReAl, RhAl, RhGa, RhHf\*\*, RhIn, RhMg, RhSc, RhY, RuAl, RuGa, RuHf, RuSc, RuTa\*, SrCd, SrHg, SrTl\*, TcHf, TcTa, TiCo, TiFe\*\*, TiIr, TiNi, TiOs, TiRe, TiRu, TiTe, TiZn, VMn, VOs, VRu\*, VTc, YIn, YTl, ZnLa, ZnSc, ZnY, ZrOs, ZrPt\*\*, ZrRu\*, ZrZn.

*B2, Pm3m, CsCl type, superoctet*

TlBr, TlCl

*B8<sub>1</sub>, P6<sub>3</sub>/mmc, NiAs type*

AuSn, CoS, CoSb, CoSe, CoTe, CrS\*, CrSb, CrSe, CrTe\*, CuGe\*, CuSn\*\*, FeS\*\*, FeSb, FeSe\*\*, FeSn\*\*, FeTe\*\*, IrPb, IrSb, IrSn, IrTe, MgPo, MnBi, MnSb, MnSn, MnTe, NiAs, NiBi, NiS\*\*, NiSb, NiSe\*\*, NiSn, NiTe\*\*, PdBi\*, PdSb, PdTe\*, PtB, PtBi, PtPb, PtSb, PtSn, PtTe, RhBi, RhSe, RhTe, ScTe, TiAs\*\*, TiP\*\*, TiS\*\*, TiSb, TiSe\*\*, TiTe, VP, VS, VSb, VSe, VTe\*\*, ZrAs\*, ZrTe, [GaS\*\* (*hP8*), GaSe\*\* (*hP8* and *hR2*), InSe\*\* (*hR2*) and InSn are superoctet systems appearing together with CuS\*\*, CuSe\*\*, and TaSe\*\* in somewhat related hexagonal structures].

*B10 (tP4)/nmm, PbO type, superoctet*

PbO\*\*, SnO\*\*

*B11, P4/nmm, CuTi type*

HfAu, PdTa, TiAu, TiCd, TiCu, ZrAg, ZrCd.

*B16, Pnma, GeS type, superoctet*

GeS, GeSe, SnS\*\*, SnSe\*\* (also InS, appearing in the related *oP8*, *Pnmm* structure. SnTe and GeTe are rhombohedral).

*B19, Pnma, AuCd type*

AuCd\*\*, MgCd, MoIr, MoPt, MoRh, NbPt, TiPb, TiPd, TiPt, VPt, WIr\*\*.

*B20, P2<sub>1</sub>3, FeSi type*

AuBe, CoSi, CrGe, CrSi, FeSi, HfSb, HfSn, MnSi, PdGa, PtAl, PtGa, PtMg, ReSi, RhSn, RuGe, RuSi\*\*, TcSi.

*B27, Pnma, FeB type*

CoB, FeB, HfB, HfGe, HfSi, LaCu, LaGe, LaSi, MnB, NiY, PtY, TiB, TiGe, TiSi, ZrGe, ZrSi\*\*.

*B31, Pnma, MnP type*

AuGa, CoAs\*\*, CoP, CrAs, CrP, FeAs, FeP, IrGe, IrSi, MnAs, MnP, MoAs, NiGe, NiSi\*\*, OsAs, OsP, PdGe, PdSi, PdSn, PtGe, PtSi, RhAs, RhGe, RhSb, RhSi\*\*, RuAs, RuP, RuSb, VAs, WP.

*B32, Fd3m, NaTl type*

LiAl, LiCd, LiGa, LiIn, LiZn\*\*, NaIn, NaTl.

*B33, Cmc, CrB type*

AgCa\*\*, AlLa\*\*, AlY, AuLa, BaGa, BaGe, BaPb, BaSi, BaSn, CaGa, CaGe, CaSi, CaSn, CrB, GaLa, GaY, HfAl, HfPt, MoB\*\*, NbB, NiB, NiHf, NiLa, NiZr, PdLa, PtLa, RhLa, ScGa, ScGe, ScSi, SrGe, SrPb, SrSi\*\*, SrSn, TaB, VB, WB\*\*, YGe, YSi, ZrAl, ZrPt.

*B35, P6/mmm, CoSn type*

CoSn, FeGe, PtTl.

*B37, I4/mcm, SeTl type, superoctet*

InTe, TlSe, TlS.

*B<sub>n</sub>P6<sub>m</sub>2, MoP type*

MoP, OsC, RuC, TaN\*\*.

*cP64, P4<sub>3</sub>n, KGe type*

CsGe, CsSi, KGe, KSi, RbGe, RbSi.

*[hP12, P6<sub>2</sub>m, NaO type]*

CaAs, CaP, KS, KSe, NaO, NaS\*\*, SrAs, SrP.

*hP24, P6<sub>3</sub>/mmc, LiO type*

LiO, NaS\*\*, NaSe.

*LI<sub>0</sub>, P4/mmm, CuAu type*

CoPt, CuAu\*\*, FeNi, FePd, FePt\*, HfAg, LiBi, MgIn, MnNi, NaBi, NbIr\*\*, NbRh\*, NiPt, PdCd, PdHg\*\*, PdMg\*, PdZn, PtCd\*, PtHg\*, PtZn\*\*, TiAg, TiAl, TiGa, TiHg, TiRh, VIr\*\*, ZrHg.

*mC24, C2/m, AsGe type, superoctet*

GaTe\*\*, GeAs, GeP, SiAs.

*mC32, C2/c, NaSi type*

NaSi.

*[mP6, P2/m, LiSn type]*

LiSn.

<i>mP16, P2<sub>1</sub>/c, LiAs type</i>	<i>[oP16, Pbca, CdSb, superoctet]</i>
KSb, LiAs, NaGe, NaSb.	CdAs, CdSb, ZnAs, ZnSb.
<i>mP32, P2<sub>1</sub>/n, NS type, superoctet</i>	<i>tI8, I4/mmm, HgCl type, superoctet</i>
AsS**, AsSe**, NS, NSe, PS**.	HgBr, HgCl, HgI.
<i>oC16, Cmcm, NaHg type</i>	<i>tI32, I4<sub>1</sub>/a, LiGe type</i>
NaHg.	LiGe.
<i>oC16, Cmca, KO type</i>	<i>[tI32, I4<sub>1</sub>/acd, NaC type</i>
KO.	KC, NaC.
<i>oC48, Cmc2<sub>1</sub>, SiP type, superoctet</i>	<i>tI32, I4/mcm, TlTe type, superoctet</i>
SiP.	TlTe.
<i>oI8, Immm, RbO type</i>	<i>tI46, I4<sub>1</sub>/acd, NaPb type</i>
CsO, CsS, RbO, RbS.	CsPb, CsSn, KPb, KSn, NaPb, RbPb, RbSn.
<i>oP16, P2<sub>1</sub>2<sub>1</sub>2<sub>1</sub>, NaP type</i>	<i>[(?), Cmcm, TlI type, superoctet]</i>
KAs, KP, NaAs, NaP, RbAs, RbP.	InBr, InI, TlI.

- <sup>1</sup>*Methods of Electronic Structure Theory*, edited by H. F. Schaefer III, in *Modern Theoretical Chemistry*, edited by W. H. Miller, H. F. Schaefer III, B. J. Berne, and G. A. Segal (Plenum, New York, 1979), Vol. 3.
- <sup>2</sup>*Applications of Electronic Structure Theory*, edited by H. F. Schaefer III, in *Modern Theoretical Chemistry*, edited by W. H. Miller, H. F. Schaefer III, B. J. Berne, and G. A. Segal (Plenum, New York, 1977), Vol. 4.
- <sup>3</sup>V. L. Moruzzi, J. F. Janak, and A. R. Williams, *Calculated Electronic Properties of Metals* (Pergamon, New York, 1978).
- <sup>4</sup>W. B. Pearson, in *Development in the Structural Chemistry of Alloy Phases*, edited by B. C. Giessen (Plenum, New York, 1969).
- <sup>5</sup>L. Pauling, *The Nature of the Chemical Bond* (Cornell University Press, Ithaca, New York, 1960).
- <sup>6</sup>W. Hume-Rothery and G. V. Raynor, *The Structure of Metals and Alloys* (Institute of Metals, London, 1957).
- <sup>7</sup>W. B. Pearson, *The Crystal Chemistry and Physics of Metal Alloys* (Wiley Interscience, New York, 1972).
- <sup>8</sup>L. S. Darken and R. W. Gurry, *Physical Chemistry of Metals* (McGraw-Hill, New York, 1953).
- <sup>9</sup>A. R. Miedema, *J. Less-Common Met.* **32**, 117 (1973); **46**, 67 (1976); A. R. Miedema, R. Boom, and F. R. DeBoer, *J. Less Common Met.* **41**, 283, (1975).
- <sup>10</sup>G. S. Pawley, *Acta Crystallogr.* **B24**, 485, (1968).
- <sup>11</sup>A. Warshel, in *Semiempirical Methods of Electronic Structure Calculations*, edited by G. A. Segal, (Plenum, New York, 1977).
- <sup>12</sup>R. Hultgren, R. D. Desai, D. T. Hawkins, H. G. Gleiser, and K. K. Kelley, *Selected Values of the Thermodynamic Properties of Binary Alloys* (American Society for Metals, Cleveland, 1973).
- <sup>13</sup>O. Kubaschewski and C. B. Alcock, *Metallurgical Thermochemistry*, 5th ed. (Pergamon, Oxford, 1979).
- <sup>14</sup>R. A. Deegan, *J. Phys. C* **1**, 763 (1968); N. W. Dalton and R. A. Deegan, *J. Phys. C* **2**, 2369 (1969).
- <sup>15</sup>J. A. Moriarty, *Phys. Rev. B* **16**, 2537 (1977).
- <sup>16</sup>J. E. Inglesfield, *Acta Metall.* **17**, 1395 (1969); *J. Phys. C* **2**, 1285 (1969); **2**, 1293 (1969).
- <sup>17</sup>J. Friedel, *The Physics of Metals*, edited by J. M. Ziman (Cambridge University Press, London, 1969).
- <sup>18</sup>M. Cyrot and F. Cyrot-Lackmann, *J. Phys. F* **6**, 2257 (1976).
- <sup>19</sup>C. H. Hodges, *J. Phys. F* **9**, L89 (1979).
- <sup>20</sup>D. G. Pettifor, *Phys. Rev. Lett* **42**, 846 (1979); *Solid State Commun.* **28**, 621 (1978).
- <sup>21</sup>C. M. Varma, *Solid State Commun.* **31**, 295 (1979).
- <sup>22</sup>J. A. Alonso and L. A. Girifalco, *Phys. Rev. B* **19**, 3889 (1979); *J. Phys. F* **8**, 2455 (1978).
- <sup>23</sup>J. C. Phillips and J. A. Van Vechten, *Phys. Rev. B* **2**, 2147 (1970); *J. C. Phillips, Rev. Mod. Phys.* **42**, 317 (1970).
- <sup>24</sup>N. Engel, *Ingenioeren* **1939**, M101.
- <sup>25</sup>N. Engel, *Acta Metall* **15**, 557 (1967).
- <sup>26</sup>L. Brewer, in *Electronic Structure and Alloy Chemistry of the Transition Elements*, edited by P. Beck (Interscience, New York, 1963), p. 221; L. Brewer, in *Phase Stability in Metals and Alloys*, edited by P. Rudman, J. Stringer, and R. I. Jaffee (McGraw-Hill, New York, 1967); L. Brewer, *Science* **161**, 115 (1968); L. Brewer and P. R. Wengert, *Metall. Trans.* **4**, 2674 (1973).
- <sup>27</sup>H. Hellman, *J. Chem. Phys.* **3**, 61 (1935a); *Acta Physicochim. URSS* **1**, 913 (1935b); H. Hellman, W. Kassatotschikin, *J. Chem. Phys.* **4**, 324 (1936); P. Gombas, *Z. Phys.* **94**, 473 (1935).
- <sup>28</sup>V. Fock, M. Vesselow, and M. Petraschen, *Zh. Eksp.*

- Theor. Fiz. 10, 723 (1940).
- <sup>29</sup>J. C. Phillips and L. Kleinman, Phys. Rev. 116, 287 (1959).
- <sup>30</sup>J. C. Phillips, *Bonds and Bands in Semiconductors* (Academic, New York, 1973).
- <sup>31</sup>M. L. Cohen and T. K. Bergstresser, Phys. Rev. 141, 739, (1966).
- <sup>32</sup>D. Brust, in *Methods in Computational Physics*, edited by B. Alder, S. Fernback, and M. Rotenberg, (Academic, New York, 1968, Vol. 8, p. 33).
- <sup>33</sup>M. L. Cohen, and V. Heine, in *Solid State Physics*, edited by H. Ehrenreich, F. Seitz, and D. Turnbull (Academic, New York, 1970, Vol. 24, p. 38).
- <sup>34</sup>W. A. Harrison, *Pseudopotentials in the Theory of Metals* (Benjamin, New York, 1966).
- <sup>35</sup>J. A. Appelbaum and D. R. Hamann, Rev. Mod. Phys. 48, 3 (1976).
- <sup>36</sup>Y. W. Yang and P. Coppens, Solid State Commun. 15, 1555 (1974).
- <sup>37</sup>D. R. Hamann, Phys. Rev. Lett. 42, 662 (1979a).
- <sup>38</sup>J. Harris and R. O. Jones, Phys. Rev. Lett. 41, 191 (1978).
- <sup>39</sup>G. Simons, J. Chem. Phys. 55, 756 (1971a); G. Simons, Chem. Phys. Lett. 12, 404 (1971b).
- <sup>40</sup>G. Simons and A. N. Bloch, Phys. Rev. B 7, 2754 (1973).
- <sup>41</sup>J. St. John and A. N. Bloch, Phys. Rev. Lett. 33, 1095 (1974).
- <sup>42</sup>E. S. Machlin, T. P. Chow, and J. C. Phillips, Phys. Rev. Lett. 38, 1292 (1977).
- <sup>43</sup>J. R. Chelikowsky and J. C. Phillips, Phys. Rev. B 17, 2453 (1978).
- <sup>44</sup>J. C. Phillips, Solid State Commun. 22, 549 (1977).
- <sup>45</sup>J. C. Phillips, Comments Solid State Phys. 9, 11 (1978).
- <sup>46</sup>A. Goldman, Phys. Status Solidi B 81, 9 (1977).
- <sup>47</sup>A. N. Bloch, unpublished results.
- <sup>48</sup>W. Andreoni, A. Baldereschi, F. Meloni, and J. C. Phillips, Solid State Commun. 24, 245 (1978).
- <sup>49</sup>W. Andreoni, A. Baldereschi, E. Biemont, and J. C. Phillips, Phys. Rev. B 20, 4814 (1979).
- <sup>50</sup>P. C. Hohenberg and W. Kohn, Phys. Rev. 136, 864 (1964).
- <sup>51</sup>W. Kohn and L. J. Sham, Phys. Rev. 140, 1133 (1965).
- <sup>52</sup>S. Topiol, A. Zunger, and M. A. Ratner, Chem. Phys. Lett. 49, 367 (1977); A. Zunger, S. Topiol, and M. A. Ratner, Chem. Phys. 39, 75 (1979).
- <sup>53</sup>A. Zunger and M. Ratner, Chem. Phys. 30, 423 (1978).
- <sup>54</sup>A. Zunger and M. L. Cohen, Phys. Rev. Lett. 41, 53 (1978).
- <sup>55</sup>A. Zunger and M. L. Cohen, Phys. Rev. B 18, 5449 (1978).
- <sup>56</sup>A. Zunger, J. Vac. Sci. Technol. 16, 1337 (1979).
- <sup>57</sup>A. Zunger, Phys. Rev. Lett. 44, 582 (1980).
- <sup>58</sup>A. Zunger and M. L. Cohen, Phys. Rev. B 20, 4082 (1979).
- <sup>59</sup>J. R. Chelikowsky and M. L. Cohen, Phys. Rev. B 14, 556 (1976).
- <sup>60</sup>M. H. Cohen and V. Heine, Phys. Rev. 122, 1821 (1961).
- <sup>61</sup>I. V. Abarenkov and V. Heine, Philos. Mag. 12, 529 (1965).
- <sup>62</sup>N. W. Ashcroft, Phys. Lett. 23, 48 (1966).
- <sup>63</sup>D. R. Hamann, M. Schlüter, and C. Chiang, Phys. Rev. Lett. 43, 1494 (1980).
- <sup>64</sup>G. P. Kerker, J. Phys. C 13, L189 (1980).
- <sup>65</sup>A. Zunger, Phys. Rev. B 22, 649 (1980); A. Zunger, J. P. Perdew, and G. Oliver, Solid State Commun. 34, 933 (1980).
- <sup>66</sup>B. I. Bennett and S. H. Vosko, Phys. Rev. B 6, 7119 (1972).
- <sup>67</sup>J. P. Walter, C. Y. Fong, and M. L. Cohen, Solid State Commun. 12, 303 (1973).
- <sup>68</sup>C. M. Bertoni, V. Bortolani, C. Calandra, and E. Nizzoli, J. Phys. F 3, L244 (1973).
- <sup>69</sup>J. Hafner, Solid State Commun. 27, 263 (1978).
- <sup>70</sup>C. H. Hodges, J. Phys. C 7, L247 (1977).
- <sup>71</sup>K. Schubert, in *Intermetallic Compounds*, edited by J. H. Westbrook (Robert E. Krieger Publishing Company, Huntington, New York, 1977), p. 100.
- <sup>72</sup>R. W. Shaw, Phys. Rev. 174, 769 (1968).
- <sup>73</sup>M. Natapoff, J. Phys. Chem. Solids 36, 53 (1975); 37, 59 (1976); 39, 1119 (1978).
- <sup>74</sup>P. Lam, M. L. Cohen, and A. Zunger, Phys. Rev. B 22, 1698 (1980).
- <sup>75</sup>N. W. Ashcroft, J. Phys. C 1, 232; N. W. Ashcroft and D. C. Langreth, Phys. Rev. 159, 500 (1967).
- <sup>76</sup>L. Szasz and G. McGinn, J. Chem. Phys. 47, 3495 (1967).
- <sup>77</sup>G. P. Kerker, A. Zunger, M. L. Cohen, and M. Schlüter, Solid State Commun. 32, 309 (1979).
- <sup>78</sup>M. Schlüter, A. Zunger, G. P. Kerker, K. M. Ho, and M. L. Cohen, Phys. Rev. Lett. 42, 540 (1979).
- <sup>79</sup>D. R. Hamann, unpublished Results.
- <sup>80</sup>A. Zunger, Phys. Rev. B 22, 959 (1980).
- <sup>81</sup>A. Zunger, G. P. Kerker, and M. L. Cohen, Phys. Rev. B 20, 581 (1979).
- <sup>82</sup>A. Zunger and M. L. Cohen, Phys. Rev. B 19, 568 (1979).
- <sup>83</sup>A. Zunger, Phys. Rev. B 21, 4785 (1980).
- <sup>84</sup>R. D. Shannon and C. T. Prewitt, Acta Crystallagr. 25B, 925 (1969).
- <sup>85</sup>C. E. Moore, *Atomic Energy Levels*, Natl. Stand. Ref. Data Ser., Natl. Bur. Stand. (U.S. GPO, Washington, D.C., 1971), Vols. 34 and 35.
- <sup>86</sup>J. C. Slater, *The Self-Consistent Field for Molecules and Solids* (McGraw-Hill, New York, 1974), p. 94.
- <sup>87</sup>W. Gordy, Phys. Rev. 69, 604 (1946).
- <sup>88</sup>E. Clementi and C. Roetti, *Atomic Data and Nuclear Data Tables* (Academic, New York, 1974), Vol. 14.
- <sup>89</sup>W. B. Pearson, *A Handbook of Lattice Spacings and Structures of Metals and Alloys* (Pergamon, Oxford, 1967), Vols. 1 and 2.
- <sup>90</sup>R. W. G. Wyckoff, *Crystal Structures*, 2nd ed. (Wiley, Interscience New York, 1963), Vols. 1-3.
- <sup>91</sup>K. Schubert, *Kristallstrukturen Zweikomponentiger Phasen* (Springer, Berlin, 1964).
- <sup>92</sup>Landolt-Börnstein, in *Structure Data of Elements and Intermetallic Phases* New Series, edited by K. H. Hellwege, A. M. Hellwege (Springer, Heidelberg, 1971), Vol. 6.
- <sup>93</sup>(a) P. M. Hansen, *Constitution of Binary Alloys* (McGraw-Hill, New York, 1958), (b) R. P. Elliot *Constitution of Binary Alloys, First Supplement* (McGraw-Hill, New York, 1965); (c) F. A. Shunk, *Constitution of Binary Alloys, Second Supplement* (McGraw-Hill, New York, 1969).
- <sup>94</sup>P. S. Rudman, J. Stringer, and R. I. Jaffe, *Phase Stability in Metals and Alloys* (McGraw-Hill, New York, 1966).
- <sup>95</sup>E. Parthé, *Crystal Chemistry of Tetrahedral Structures* (Gordon and Breach, New York, 1964).

- <sup>96</sup>W. Rieger and E. Parthé, *Acta Crystallogr.* 22, 919 (1966).
- <sup>97</sup>O. Schob, and E. Parthé, *Acta Crystallogr.* 19, 214 (1964).
- <sup>98</sup>(a) D. Hohnke and E. Parthé, *Acta Crystallogr.* 20, 572 (1965); (b) S. C. Panda and S. Bhn, *Z. Mettalk.* 64, 126 (1973); 64, 793 (1973).
- <sup>99</sup>K. Schubert and P. Eslinger, *Z. Mettalk.* 48, 126 (1957); 48, 193 (1957).
- <sup>100</sup>M. Barber, J. W. Linnett, and M. Taylor, *J. Chem. Soc.* 1961, 3323.
- <sup>101</sup>(a) W. Jeitscko, private communication; (b) F. Hulliger, private communication. Also see comment in Ref. 89, p. 56.
- <sup>102</sup>A. Navrotsky and J. C. Phillips, *Phys. Rev. B* 11, 1583 (1975).
- <sup>103</sup>M. B. Brodsky and J. O. Brittain, *J. Appl. Phys.* 40, 3615 (1969); D. A. Kiewit and J. O. Brittain, *ibid.* 41, 710 (1970).
- <sup>104</sup>(a) R. Herget, E. Wreser, H. Gengnagel, and A. Gladun, *Phys. Status Solidi* 41, 255 (1970); (b) J. Bras, J. J. Couderc, M. Fagot, and J. Ferre, *Acta Metall.* 25, 1077 (1977).
- <sup>105</sup>G. K. Wertheim and J. H. Wernick, *Acta Metall.* 15, 297 (1967).
- <sup>106</sup>G. P. Huffman, *J. Appl. Phys.* 42, 1606 (1971).
- <sup>107</sup>A. Bose, G. Froberg, and H. Wever, *Phys. Status Solidi A* 52, 509 (1979).
- <sup>108</sup>V. Gerold, *J. Appl. Crystallogr.* 11, 153 (1978).
- <sup>109</sup>M. W. Meisel, W. P. Halperin, Y. Ochiani, and J. O. Brittain, *J. Phys. F* 10, L105 (1980).
- <sup>110</sup>D. J. Sellmyer, G. R. Caskey, and J. Franz, *J. Phys. Chem. Solids* 33, 561 (1971).
- <sup>111</sup>K. J. Best, H. J. Rodies, and H. Jacobi, *Z. Mettalk.* 62, 634 (1971).
- <sup>112</sup>R. E. Marsh and D. P. Shoemaker, *Acta Crystallogr.* 6, 197 (1953); I. F. Hewaidy, E. Busmann, and W. Klein, *Z. Anorg. Allg. Chem.* 328, 283 (1964).
- <sup>113</sup>R. st. Amand and B. C. Giessen, *Scr. Metall.* 12, 1021 (1978).
- <sup>114</sup>P. Eurin and J. Pauleve, *IEEE Trans. Magn.* 3, 216 (1969).
- <sup>115</sup>N. N. Evtikhiev, N. A. Ekonomov, A. R. Krebs, N. A. Zamyatina, A. S. Komalov, V. G. Pinko, and L. V. Iraeva, *Phys. Status Solidi A* 50, K153 (1978).
- <sup>116</sup>G. V. Ivanova, L. M. Magat, L. V. Solina, and Y. S. Shur, *Fiz. Met. Metalloved.* 32, 543 (1971) [*Phys. Met. Metallogr. (USSR)* 32, 92 (1971)].
- <sup>117</sup>G. V. Ivanova and L. M. Magat, *Fiz. Met. Metalloved.* 39, 999 (1975) [*Phys. Met. Metallogr. (USSR)* 39, 88 (1971)].
- <sup>118</sup>W. E. Spicer, *Phys. Rev.* 125, 1297 (1962); A. Sommer, *Nature (London)* 152, 215 (1943).
- <sup>119</sup>A. Hasegawa, M. Watabe, *J. Phys. F* 7, 75, (1977).
- <sup>120</sup>P. Littelwood, *J. Phys. C* 12, 4441 (1979).
- <sup>121</sup>A. R. Williams, J. Kübler, C. D. Gelatt, *Phys. Rev. B* 19, 6094 (1979).
- <sup>122</sup>T. Anno, *J. Chem. Phys.* 69, 5213 (1978).
- <sup>123</sup>K. Rudenberg, *J. Chem. Phys.* 66, 375 (1977).
- <sup>124</sup>P. Politzer, *J. Chem. Phys.* 64, 4239 (1976).
- <sup>125</sup>K. D. Sen, *J. Phys. B* 12, L287 (1979).
- <sup>126</sup>J. F. Mucci and N. H. March, *J. Chem. Phys.* 71, 1495 (1979).
- <sup>127</sup>A. Francois and L. Pujol, *J. Chem. Phys.* 71, 1066 (1979).
- <sup>128</sup>T. Anno, *J. Chem. Phys.* 72, 782 (1980).
- <sup>129</sup>C. V. R. Rao and K. D. Sen, *J. Chem. Phys.* 70, 586 (1979).
- <sup>130</sup>D. J. Chadi, *Phys. Rev. Lett.* 41, 1062 (1978); *Phys. Rev. B* 19, 2074 (1979).
- <sup>131</sup>D. Hackenbracht and J. Kübler, *J. Phys. F* 10, 427 (1980).
- <sup>132</sup>A. R. Williams, C. D. Gelatt, and V. L. Moruzzi, *Phys. Rev. Lett.* 44, 429 (1980).
- <sup>133</sup>A. Zunger and A. J. Freeman, *Phys. Rev. B* 16, 2901 (1977); 17, 4850 (1978).
- <sup>134</sup>K. S. Pitzer, *J. Am. Chem. Soc.* 70, 2140 (1948).